spotlight the germline rules for alphabeta T cell-receptor interactions with MHC molecules. Immunity *28*, 324–334.

Derbinski, J., Schulte, A., Kyewski, B., and Klein, L. (2001). Promiscuous gene expression in medullary thymic epithelial cells mirrors the peripheral self. Nat. Immunol. *2*, 1032–1039.

Doherty, P.C., Topham, D.J., Tripp, R.A., Cardin, R.D., Brooks, J.W., and Stevenson, P.G. (1997). Effector $CD4^+$ and $CD8^+$ T-cell mechanisms in the control of respiratory virus infections. Immunol. Rev. *159*, 105–117.

Ernst, B., Lee, D.S., Chang, J.M., Sprent, J., and Surh, C.D. (1999). The peptide ligands mediating positive selection in the thymus control T cell survival and homeostatic proliferation in the periphery. Immunity *11*, 173–181.

Falk, K., Rötzschke, O., Stevanović, S., Jung, G., and Rammensee, H.G. (1991). Allele-specific motifs revealed by sequencing of self-peptides eluted from MHC molecules. Nature *351*, 290–296.

Fehling, H.J., Swat, W., Laplace, C., Kühn, R., Rajewsky, K., Müller, U., and von Boehmer, H. (1994). MHC class I expression in mice lacking the proteasome subunit LMP-7. Science *265*, 1234–1237.

Fukui, Y., Ishimoto, T., Utsuyama, M., Gyotoku, T., Koga, T., Nakao, K., Hirokawa, K., Katsuki, M., and Sasazuki, T. (1997). Positive and negative $CD4^+$ thymocyte selection by a single MHC class II/peptide ligand affected by its expression level in the thymus. Immunity *6*, 401–410.

Ge, Q., Bai, A., Jones, B., Eisen, H.N., and Chen, J. (2004). Competition for self-peptide-MHC complexes and cytokines between naive and memory $CD8^+$ T cells expressing the same or different T cell receptors. Proc. Natl. Acad. Sci. USA *101*, 3041–3046.

Gommeaux, J., Grégoire, C., Nguessan, P., Richelme, M., Malissen, M., Guerder, S., Malissen, B., and Carrier, A. (2009). Thymus-specific serine protease regulates positive selection of a subset of $CD4^+$ thymocytes. Eur. J. Immunol. *39*, 956–964.

Gray, D.H., Seach, N., Ueno, T., Milton, M.K., Liston, A., Lew, A.M., Goodnow, C.C., and Boyd, R.L. (2006). Developmental kinetics, turnover, and stimulatory capacity of thymic epithelial cells. Blood *108*, 3777–3785.

Heinemeyer, W., Gruhler, A., Möhrle, V., Mahé, Y., and Wolf, D.H. (1993). PRE2, highly homologous to the human major histocompatibility complex-linked RING10 gene, codes for a yeast proteasome subunit necessary for chrymotryptic activity and degradation of ubiquitinated proteins. J. Biol. Chem. *268*, 5115–5120.

Hikosaka, Y., Nitta, T., Ohigashi, I., Yano, K., Ishimaru, N., Hayashi, Y., Matsumoto, M., Matsuo, K., Penninger, J.M., Takayanagi, H., et al. (2008). The cytokine RANKL produced by positively selected thymocytes fosters medullary thymic epithelial cells that express autoimmune regulator. Immunity *29*, 438–450.

Hogquist, K.A., Jameson, S.C., Heath, W.R., Howard, J.L., Bevan, M.J., and Carbone, F.R. (1994). T cell receptor antagonist peptides induce positive selection. Cell *76*, 17–27.

Honey, K., Nakagawa, T., Peters, C., and Rudensky, A. (2002). Cathepsin L regulates $CD4^+$ T cell selection independently of its effect on invariant chain: a role in the generation of positively selecting peptide ligands. J. Exp. Med. *195*, 1349–1358.

Hugo, P., Kappler, J.W., McCormack, J.E., and Marrack, P. (1993). Fibroblasts can induce thymocyte positive selection in vivo. Proc. Natl. Acad. Sci. USA *90*, 10335–10339.

Hunt, D.F., Henderson, R.A., Shabanowitz, J., Sakaguchi, K., Michel, H., Sevilir, N., Cox, A.L., Appella, E., and Engelhard, V.H. (1992). Characterization of peptides bound to the class I MHC molecule HLA-A2.1 by mass spectrometry. Science *255*, 1261–1263.

Huseby, E.S., White, J., Crawford, F., Vass, T., Becker, D., Pinilla, C., Marrack, P., and Kappler, J.W. (2005). How the T cell repertoire becomes peptide and MHC specific. Cell *122*, 247–260.

Huseby, E.S., Kappler, J.W., and Marrack, P. (2008). Thymic selection stifles TCR reactivity with the main chain structure of MHC and forces interactions with the peptide side chains. Mol. Immunol. *45*, 599–606.

Ignatowicz, L., Kappler, J., and Marrack, P. (1996). The repertoire of T cells shaped by a single MHC/peptide ligand. Cell *84*, 521–529.

Kappler, J.W., Roehm, N., and Marrack, P. (1987). T cell tolerance by clonal elimination in the thymus. Cell *49*, 273–280.

Kedzierska, K., Venturi, V., Field, K., Davenport, M.P., Turner, S.J., and Doherty, P.C. (2006). Early establishment of diverse T cell receptor profiles for influenza-specific $CD8(^+)CD62L(^{hi})$ memory T cells. Proc. Natl. Acad. Sci. USA *103*, 9184–9189.

Kirberg, J., Bosco, N., Deloulme, J.C., Ceredig, R., and Agenès, F. (2008). Peripheral T lymphocytes recirculating back into the thymus can mediate thymocyte positive selection. J. Immunol. *181*, 1207–1214.

Kisielow, P., Teh, H.S., Blüthmann, H., and von Boehmer, H. (1988). Positive selection of antigen-specific T cells in thymus by restricting MHC molecules. Nature *335*, 730–733.

Kurobe, H., Liu, C., Ueno, T., Saito, F., Ohigashi, I., Seach, N., Arakaki, R., Hayashi, Y., Kitagawa, T., Lipp, M., et al. (2006). CCR7-dependent cortex-to-medulla migration of positively selected thymocytes is essential for establishing central tolerance. Immunity *24*, 165–177.

Kyewski, B., and Derbinski, J. (2004). Self-representation in the thymus: an extended view. Nat. Rev. Immunol. *4*, 688–698.

Li, W., Kim, M.G., Gourley, T.S., McCarthy, B.P., Sant'Angelo, D.B., and Chang, C.H. (2005). An alternate pathway for CD4 T cell development: thymocyte-expressed MHC class II selects a distinct T cell population. Immunity *23*, 375–386.

Li, J., Iwanami, N., Hoa, V.Q., Furutani-Seiki, M., and Takahama, Y. (2007). Noninvasive intravital imaging of thymocyte dynamics in medaka. J. Immunol. *179*, 1605–1615.

Lie, W.R., Myers, N.B., Connolly, J.M., Gorka, J., Lee, D.R., and Hansen, T.H. (1991). The specific binding of peptide ligand to $L^d$ class I major histocompatibility complex molecules determines their antigenic structure. J. Exp. Med. *173*, 449–459.

Lilić, M., Santori, F.R., Neilson, E.G., Frey, A.B., and Vukmanović, S. (2002). The role of fibroblasts in thymocyte-positive selection. J. Immunol. *169*, 4945–4950.

Mareeva, T., Martinez-Hackert, E., and Sykulev, Y. (2008). How a T cell receptor-like antibody recognizes major histocompatibility complex-bound peptide. J. Biol. Chem. *283*, 29053–29059.

Marrack, P., and Kappler, J. (1997). Positive selection of thymocytes bearing $\alpha\,\beta$ T cell receptors. Curr. Opin. Immunol. *9*, 250–255.

Martinic, M.M., Rülicke, T., Althage, A., Odermatt, B., Höchli, M., Lamarre, A., Dumrese, T., Speiser, D.E., Kyburz, D., Hengartner, H., and Zinkernagel, R.M. (2003). Efficient T cell repertoire selection in tetraparental chimeric mice independent of thymic epithelial MHC. Proc. Natl. Acad. Sci. USA *100*, 1861–1866.

Merkenschlager, M., Graf, D., Lovatt, M., Bommhardt, U., Zamoyska, R., and Fisher, A.G. (1997). How many thymocytes audition for selection? J. Exp. Med. *186*, 1149–1158.

Momburg, F., Roelse, J., Howard, J.C., Butcher, G.W., Hämmerling, G.J., and Neefjes, J.J. (1994). Selectivity of MHC-encoded peptide transporters from human, mouse and rat. Nature *367*, 648–651.

Mozdzanowska, K., Furchner, M., Maiese, K., and Gerhard, W. (1997). $CD4^+$ T cells are ineffective in clearing a pulmonary infection with influenza type A virus in the absence of B cells. Virology *239*, 217–225.

Murali-Krishna, K., Lau, L.L., Sambhara, S., Lemonnier, F., Altman, J., and Ahmed, R. (1999). Persistence of memory CD8 T cells in MHC class I-deficient mice. Science *286*, 1377–1381.

Murata, S., Sasaki, K., Kishimoto, T., Niwa, S., Hayashi, H., Takahama, Y., and Tanaka, K. (2007). Regulation of $CD8^+$ T cell development by thymus-specific proteasomes. Science *316*, 1349–1353.

Nakagawa, T., Roth, W., Wong, P., Nelson, A., Farr, A., Deussing, J., Villadangos, J.A., Ploegh, H., Peters, C., and Rudensky, A.Y. (1998). Cathepsin L: critical role in Ii degradation and CD4 T cell selection in the thymus. Science *280*, 450–453.

Nedjic, J., Aichinger, M., Emmerich, J., Mizushima, N., and Klein, L. (2008). Autophagy in thymic epithelium shapes the T-cell repertoire and is essential for tolerance. Nature *455*, 396–400.

Nitta, T., Nitta, S., Lei, Y., Lipp, M., and Takahama, Y. (2009). CCR7-mediated migration of developing thymocytes to the medulla is essential for negative selection to tissue-restricted antigens. Proc. Natl. Acad. Sci. USA *106*, 17129–17133.

Oono, T., Fukui, Y., Masuko, S., Hashimoto, O., Ueno, T., Sanui, T., Inayoshi, A., Noda, M., Sata, M., and Sasazuki, T. (2001). Organ-specific autoimmunity in mice whose T cell repertoire is shaped by a single antigenic peptide. J. Clin. Invest. *108*, 1589–1596.

Palmer, E. (2003). Negative selection—clearing out the bad apples from the T-cell repertoire. Nat. Rev. Immunol. *3*, 383–391.

Park, J.H., Adoro, S., Lucas, P.J., Sarafova, S.D., Alag, A.S., Doan, L.L., Erman, B., Liu, X., Ellmeier, W., Bosselut, R., et al. (2007). 'Coreceptor tuning': cytokine signals transcriptionally tailor CD8 coreceptor expression to the self-specificity of the TCR. Nat. Immunol. *8*, 1049–1059.

Pawlowski, T., Elliott, J.D., Loh, D.Y., and Staerz, U.D. (1993). Positive selection of T lymphocytes on fibroblasts. Nature *364*, 642–645.

Porgador, A., Yewdell, J.W., Deng, Y., Bennink, J.R., and Germain, R.N. (1997). Localization, quantitation, and in situ detection of specific peptide-MHC class I complexes using a monoclonal antibody. Immunity *6*, 715–726.

Reits, E., Griekspoor, A., Neijssen, J., Groothuis, T., Jalink, K., van Veelen, P., Janssen, H., Calafat, J., Drijfhout, J.W., and Neefjes, J. (2003). Peptide diffusion, protection, and degradation in nuclear and cytoplasmic compartments before antigen presentation by MHC class I. Immunity *18*, 97–108.

Rock, K.L., and Goldberg, A.L. (1999). Degradation of cell proteins and the generation of MHC class I-presented peptides. Annu. Rev. Immunol. *17*, 739–779.

Rock, K.L., Gramm, C., Rothstein, L., Clark, K., Stein, R., Dick, L., Hwang, D., and Goldberg, A.L. (1994). Inhibitors of the proteasome block the degradation of most cell proteins and the generation of peptides presented on MHC class I molecules. Cell *78*, 761–771.

Scollay, R., Wilson, A., D'Amico, A., Kelly, K., Egerton, M., Pearse, M., Wu, L., and Shortman, K. (1988). Developmental status and reconstitution potential of subpopulations of murine thymocytes. Immunol. Rev. *104*, 81–120.

Sebzda, E., Wallace, V.A., Mayer, J., Yeung, R.S., Mak, T.W., and Ohashi, P.S. (1994). Positive and negative thymocyte selection induced by different concentrations of a single peptide. Science *263*, 1615–1618.

Siggs, O.M., Makaroff, L.E., and Liston, A. (2006). The why and how of thymocyte negative selection. Curr. Opin. Immunol. *18*, 175–183.

Singer, A., Mizuochi, T., Munitz, T.I., and Gress, R.E. (1986). Role of self antigen in the selection of the developing T cell repertoire. Prog Immunol. *6*, 60–66.

Stambas, J., Doherty, P.C., and Turner, S.J. (2007). An *in vivo* cytotoxicity threshold for influenza A virus-specific effector and memory CD8(+) T cells. J. Immunol. *178*, 1285–1292.

Starr, T.K., Jameson, S.C., and Hogquist, K.A. (2003). Positive and negative selection of T cells. Annu. Rev. Immunol. *21*, 139–176.

Strasser, A. (2005). The role of BH3-only proteins in the immune system. Nat. Rev. Immunol. *5*, 189–200.

Takahama, Y. (2006). Journey through the thymus: stromal guides for T-cell development and selection. Nat. Rev. Immunol. *6*, 127–135.

Takahama, Y., Suzuki, H., Katz, K.S., Grusby, M.J., and Singer, A. (1994). Positive selection of $CD4^+$ T cells by TCR ligation without aggregation even in the absence of MHC. Nature *371*, 67–70.

Takahama, Y., Tanaka, K., and Murata, S. (2008). Modest cortex and promiscuous medulla for thymic repertoire formation. Trends Immunol. *29*, 251–255.

Tanchot, C., Lemonnier, F.A., Pérarnau, B., Freitas, A.A., and Rocha, B. (1997). Differential requirements for survival and proliferation of CD8 naïve or memory T cells. Science *276*, 2057–2062.

Uebel, S., Kraas, W., Kienle, S., Wiesmüller, K.H., Jung, G., and Tampé, R. (1997). Recognition principle of the TAP transporter disclosed by combinatorial peptide libraries. Proc. Natl. Acad. Sci. USA *94*, 8976–8981.

Ueno, T., Liu, C., Nitta, T., and Takahama, Y. (2005). Development of T-lymphocytes in mouse fetal thymus organ culture. Methods Mol. Biol. *290*, 117–133.

von Boehmer, H. (1994). Positive selection of lymphocytes. Cell *76*, 219–228.

Yewdell, J.W., Reits, E., and Neefjes, J. (2003). Making sense of mass destruction: quantitating MHC class I antigen presentation. Nat. Rev. Immunol. *3*, 952–961.

Young, A.C., Nathenson, S.G., and Sacchettini, J.C. (1995). Structural studies of class I major histocompatibility complex proteins: insights into antigen presentation. FASEB J. *9*, 26–36.

Zerrahn, J., Held, W., and Raulet, D.H. (1997). The MHC reactivity of the T cell repertoire prior to positive and negative selection. Cell *88*, 627–636.

Zerrahn, J., Volkmann, A., Coles, M.C., Held, W., Lemonnier, F.A., and Raulet, D.H. (1999). Class I MHC molecules on hematopoietic cells can support intrathymic positive selection of T cell receptor transgenic T cells. Proc. Natl. Acad. Sci. USA *96*, 11470–11475.

Zinkernagel, R.M., and Althage, A. (1999). On the role of thymic epithelium vs. bone marrow-derived cells in repertoire selection of T cells. Proc. Natl. Acad. Sci. USA *96*, 8092–8097.

Zinkernagel, R.M., Callahan, G.N., Althage, A., Cooper, S., Klein, P.A., and Klein, J. (1978). On the thymus in the differentiation of "H-2 self-recognition" by T cells: evidence for dual recognition? J. Exp. Med. *147*, 882–896.

nature cell biology

# The selective autophagy substrate p62 activates the stress responsive transcription factor Nrf2 through inactivation of Keap1

Masaaki Komatsu[1,2,8], Hirofumi Kurokawa[3], Satoshi Waguri[4], Keiko Taguchi[3], Akira Kobayashi[5], Yoshinobu Ichimura[1,6], Yu-Shin Sou[1,6], Izumi Ueno[1], Ayako Sakamoto[1], Kit I. Tong[3], Mihee Kim[5], Yasumasa Nishito[1], Shun-ichiro Iemura[7], Tohru Natsume[7], Takashi Ueno[6], Eiki Kominami[6], Hozumi Motohashi[3], Keiji Tanaka[1,8] and Masayuki Yamamoto[3,8]

**Impaired selective turnover of p62 by autophagy causes severe liver injury accompanied by the formation of p62-positive inclusions and upregulation of detoxifying enzymes. These phenotypes correspond closely to the pathological conditions seen in human liver diseases, including alcoholic hepatitis and hepatocellular carcinoma. However, the molecular mechanisms and pathophysiological processes in these events are still unknown. Here we report the identification of a novel regulatory mechanism by p62 of the transcription factor Nrf2, whose target genes include antioxidant proteins and detoxification enzymes. p62 interacts with the Nrf2-binding site on Keap1, a component of Cullin-3-type ubiquitin ligase for Nrf2. Thus, an overproduction of p62 or a deficiency in autophagy competes with the interaction between Nrf2 and Keap1, resulting in stabilization of Nrf2 and transcriptional activation of Nrf2 target genes. Our findings indicate that the pathological process associated with p62 accumulation results in hyperactivation of Nrf2 and delineates unexpected roles of selective autophagy in controlling the transcription of cellular defence enzyme genes.**

Macroautophagy (hereafter referred to as autophagy) is a highly conserved bulk protein degradation pathway responsible for the turnover of long-lived proteins, the disposal of excess or damaged organelles, and the clearance of aggregation-prone proteins. Isolation membranes engulf the cytoplasmic constituents, and the resulting autophagosomes fuse with lysosomes, resulting in complete degradation of the sequestered cytoplasmic components by lysosomal hydrolases[1]. Thus, inactivation of autophagy leads to cytoplasmic protein inclusions, which are composed of degenerated proteins, and the excess accumulation of deformed organelles, leading to liver injury[2], diabetes[3,4], heart disease[5] and neurodegeneration[6,7].

Although autophagy has generally been considered non-selective, growing lines of evidence indicate the selectivity of autophagy in sorting vacuolar enzymes such as aminopeptidase I and α-mannosidase[8] and in the removal of aggregation-prone proteins[9], unwanted organelles[10,11], and microbes[12]. Such selectivity by autophagy enables various methods of cellular regulation, as is well known for the ubiquitin proteasome pathway. The protein p62, which binds ubiquitin and LC3 (refs 13–15) and is a selective substrate for autophagy, regulates the formation of protein aggregates. Genetic ablation of *p62* suppressed the appearance of ubiquitin-positive protein aggregates in autophagy-deficient mice[16] and flies[17], indicating that p62 is important in the formation of inclusion bodies. Moreover, loss of *p62* markedly attenuated liver injury accompanied by the robust induction of antioxidant proteins resulting from autophagy deficiency[16]. This implies that impaired turnover of p62 is a major cause of the pathogenic changes seen in the livers of autophagy-deficient mice. Importantly, excess accumulation of p62 and inclusion bodies containing both ubiquitylated proteins and p62 have been identified in several human disorders, especially in neurodegenerative diseases[18], liver injuries[19] and hepatocellular carcinoma[20]. However, the molecular functions of p62 in autophagy-deficient conditions and its pathophysiological roles in human disorders are still unknown.

The Nrf2–Keap1 system is currently recognized as one of the main cellular defence mechanisms against oxidative and electrophilic stresses[21–23]. Under quiescent conditions, the transcription factor Nrf2 (nuclear factor erythroid 2-related factor 2) is constitutively degraded through the ubiquitin–proteasome pathway because its binding partner Keap1

[1]Laboratory of Frontier Science, Tokyo Metropolitan Institute of Medical Science, Bunkyo-ku, Tokyo 113-8613, Japan. [2]PRESTO, Japan Science and Technology Corporation, Kawaguchi 332-0012, Japan. [3]Department of Medical Biochemistry and ERATO-JST, Tohoku University Graduate School of Medicine, Aoba-ku, Sendai 980-8575, Japan. [4]Department of Anatomy and Histology, Fukushima Medical University School of Medicine, Hikarigaoka, Fukushima 960-1295, Japan. [5]Department of Medical Life Systems, Doshisha University, Kyoutanabe, Kyoto 610-0394, Japan. [6]Department of Biochemistry, Juntendo University School of Medicine, Bunkyo-ku, Tokyo 113-8421, Japan. [7]National Institutes of Advanced Industrial Science and Technology, Biological Information Research Center (JBIRC), Kohtoh-ku, Tokyo 135-0064, Japan.
[8]Correspondence should be addressed to M.K., K.T. or M.Y. (e-mail: komatsu-ms@igakuken.or.jp; tanaka-kj@igakuken.or.jp; masiyamamoto@m.tains.tohoku.ac.jp).

Received 19 November 2009; accepted 1 February 2010; published online 21 February 2010; DOI:10.1038/ncb2021

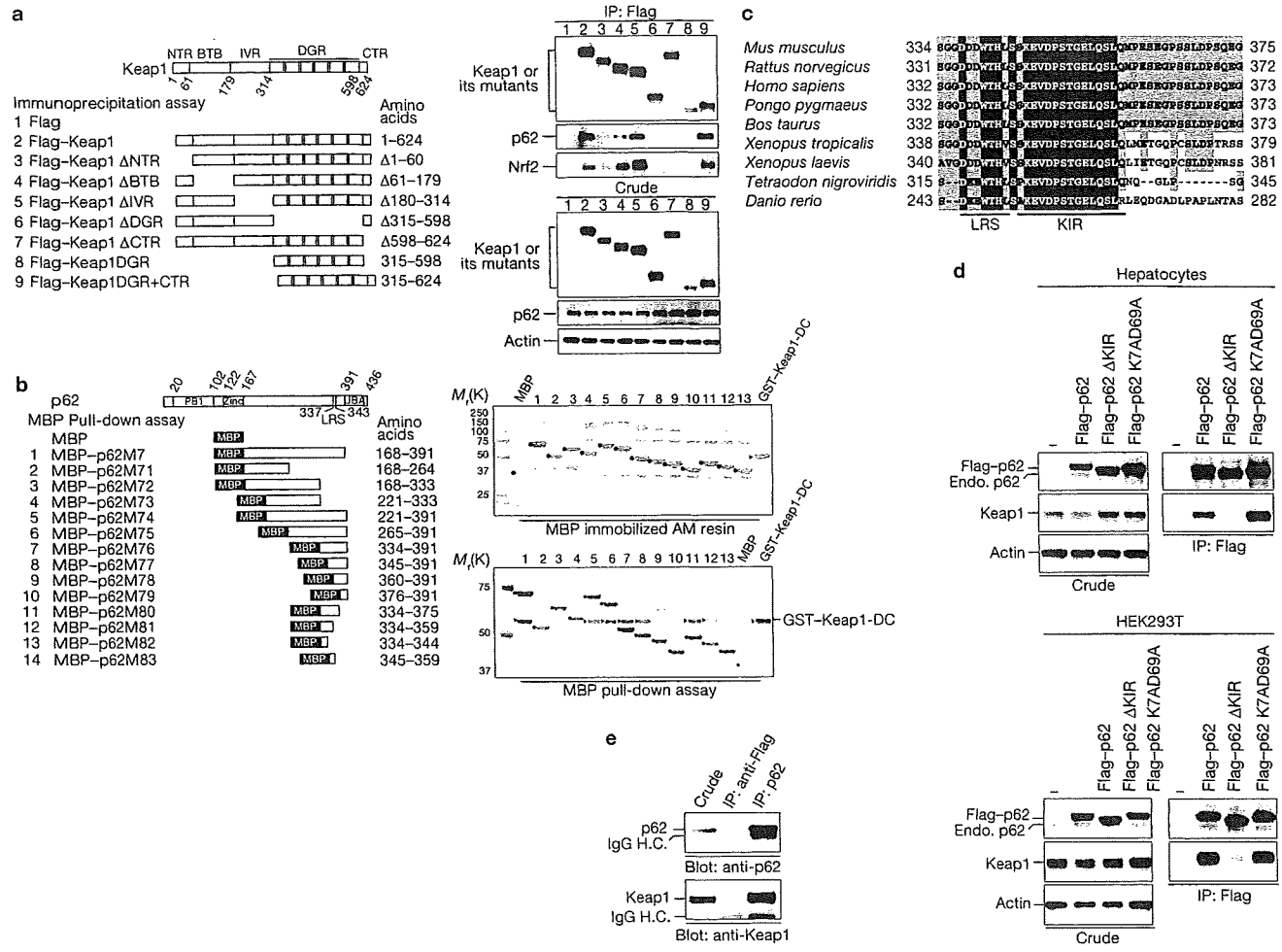


**Figure 1** Interaction between Keap1 and p62. (**a**) Diagrams of the deletion–mutation constructs of Keap1 (left) and the corresponding immunoprecipitation assays (right). Each Flag-tagged mouse Keap1 and mutant was expressed in HEK293T cells. At 22 h after transfection, lysates were prepared and immunoprecipitated with anti-Flag antibody. The resulting immunoprecipitates were subjected to SDS–PAGE and analysed by immunoblotting with anti-Flag, anti-p62, anti-Nrf2 and anti-actin antibodies. Data are representative of three individual experiments. (**b**) Diagrams of the deletion–mutation constructs of p62 (left) and the corresponding input (upper right) and pull-down assay (lower right). The MBP-tagged mouse p62 deletion mutants conjugated to amylose (AM) resins were incubated with purified GST-tagged mouse Keap1-DC. The pulled-down complexes with the MBP–p62 mutants were subjected to SDS–PAGE and revealed by staining with Coomassie brilliant blue. The bands corresponding to MBP–p62 and its mutants are indicated by black dots. Red arrowheads indicate the band corresponding to GST–Keap1-DC. For details of construct 14 see Supplementary Information, Fig. S3. (**c**) Alignment of the Keap1-interacting regions (KIR; red line) and the LC3-recognition sequences (LRS; green line) of p62 homologues in various species. Black and grey boxes indicate identical amino acid residues with complete and partial conservation, respectively. (**d**) Immunoprecipitation assays. Flag-tagged p62, KIR-deleted p62 (p62 ΔKIR) and a p62 mutant defective in oligomerization (p62 K7AD69A) were expressed in primary mouse hepatocytes by the adenovirus system (left) or in HEK293T cells by transfection (right). Cell lysates were immunoprecipitated with anti-Flag antibody. The resulting immunoprecipitates were subjected to SDS–PAGE and analysed by immunoblotting with anti-p62 and anti-Keap1 antibodies. The bands corresponding to Flag–p62, endogenous p62, Keap1 and actin are indicated. The data shown are representative of three separate experiments. (**e**) Interaction of endogenous p62 with Keap1. Lysates prepared from the human hepatocellular carcinoma cell line Huh-1 were immunoprecipitated with anti-p62 antibody or anti-Flag antibody (negative control) followed by immunoblotting with antibodies against p62 and Keap1. The bands corresponding to endogenous p62, Keap1 and IgG heavy chain (IgG H.C.) are indicated. The data shown are representative of three separate experiments. Uncropped images of blots are shown in Supplementary Information, Fig. S11.

(kelch-like ECH-associated protein 1) is an adaptor of the ubiquitin ligase complex[24–27]. Exposure to electrophiles, reactive oxygen species and nitric oxide instigates the modification of the cysteine residues of Keap1, leading to its inactivation[28–30]. As a result, Nrf2 becomes stabilized and translocates to the nucleus to induce the transcription of numerous cytoprotective genes through its heterodimerization with small Maf proteins[31–33] (see Supplementary Information, Fig. S10). In this study we found that p62 acts to stabilize Nrf2 in autophagy-deficient mouse livers and subsequently induces the expression of various cytoprotective enzymes. This sustained activation of Nrf2 seems to be a major cause of toxicity in autophagy-impaired livers.

## RESULTS

### Identification of Keap1 as a p62-interacting protein

Previous genetic studies on the autophagy-essential protein Atg7 in the mouse showed that loss of autophagy caused a marked accumulation

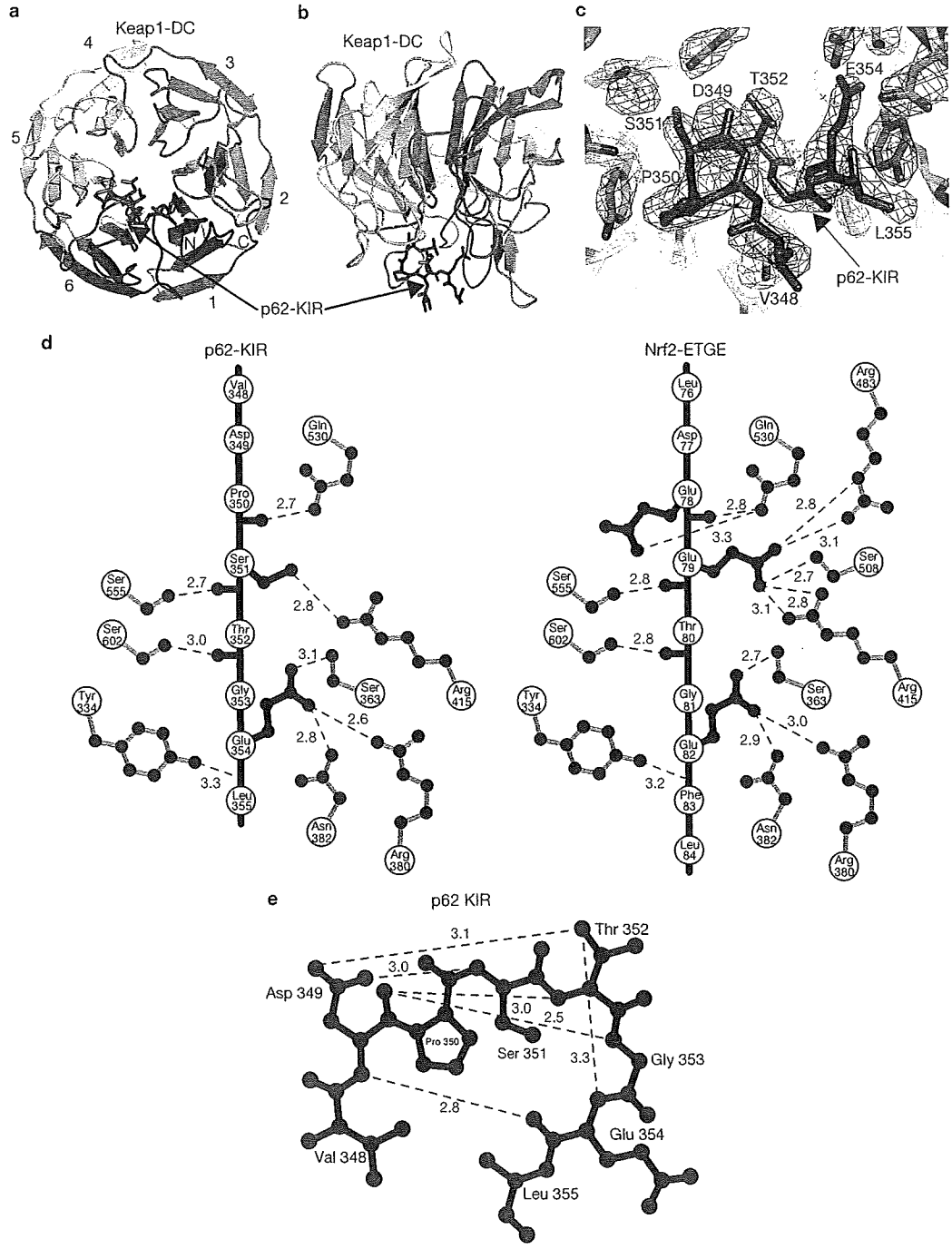


**Figure 2** Crystal structure of Keap1-DC in complex with p62-KIR. (**a**, **b**) Bottom view (**a**) and side view (**b**) of the complex structure. The ribbon model represents Keap1-DC and the stick model shows p62-KIR. Each β-propeller blade is numbered from 1 to 6. (**c**) The simulated-annealing $F_o - F_c$ omit map is contoured at 3 σ. p62-KIR (pink) was omitted from the calculation. The electron density of the peptide-bound region V348 to L355 of p62-KIR was unambiguously visible. (**d**) Intermolecular hydrogen bonds of Keap1-DC in complex with p62-KIR (left; PDB ID 3ADE) and in complex with the Nrf2-ETGE region (right; PDB ID 1x2r). (**e**) Intra-peptide hydrogen bonds of p62-KIR in the Keap1-DC complex. Hydrogen bonds (green broken lines) and their distances (Å) are displayed in **d** and **e**.

of p62 along with robust induction of antioxidant proteins, including NAD(P)H dehydrogenase quinone 1 (Nqo1) and glutathione *S*-transferase (GST)[16]. A battery of such detoxifying and antioxidant genes is regulated by the transcription factor Nrf2, which is activated by oxidative and electrophilic stresses[31,32] (see Supplementary Information, Fig. S10). A prominent accumulation of Nrf2 in the nucleus was observed in livers deficient in Atg7, but this was ameliorated by the additional loss of p62 (ref. 16). We therefore postulated that in autophagy-deficient livers, oxidative stresses occur in a p62-dependent manner. However, treatment of *Atg7*-deficient hepatocytes with the antioxidant reagent *N*-acetylcysteine did not affect the nuclear accumulation of Nrf2 or the high-level expression of antioxidant enzymes (Supplementary

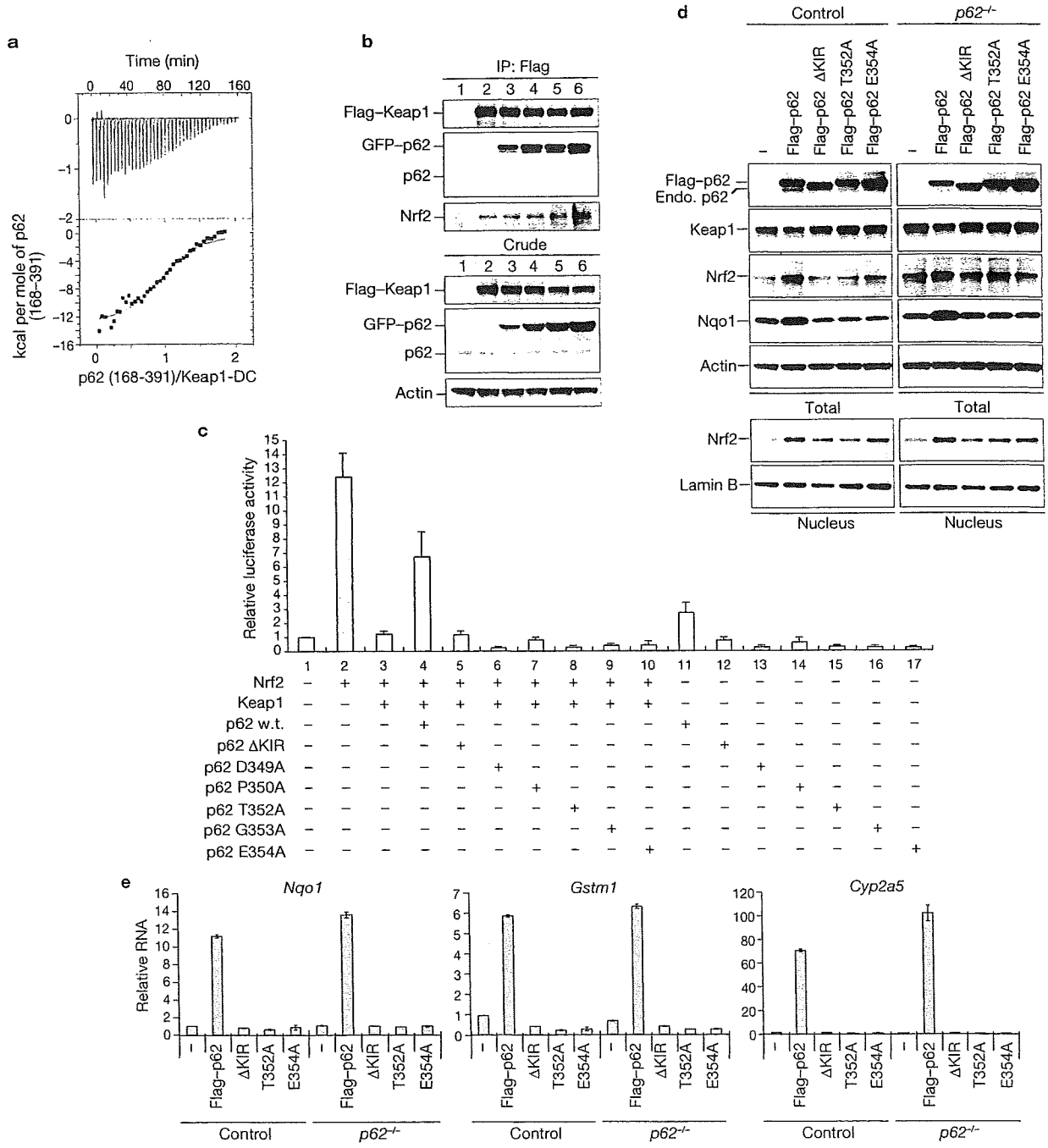


**Figure 3** Competitive inhibition of the Nrf2–Keap1 pathway by p62. **(a)** A representative ITC profile of the titration of Keap1-DC with p62M7 (residues 168–391). The upper panel shows the raw ITC thermograms and the lower panel shows the fitted binding isotherms. **(b)** Immunoprecipitation assays. Flag-tagged Keap1 was co-expressed with increasing concentrations of green fluorescent protein (GFP)–p62 (lanes 3–6) in HEK293T cells. Cell lysates were immunoprecipitated with anti-Flag antibody. The resulting immunoprecipitates were subjected to SDS–PAGE and analysed by immunoblotting with anti-Flag, anti-p62 and anti-Nrf2 antibodies. The bands corresponding to Flag–Keap1, endogenous p62, Nrf2 and actin are indicated. Data are representative of three independent experiments. **(c)** The competitive p62 activity against Keap1 was measured by luciferase assay. The expression plasmids for Nrf2, Keap1 and p62 wild-type (w.t.) or its mutants were transfected into Hepa1 cells along with pNqo1-ARE reporter plasmid and pRL-TK as an internal control. At 36 h after transfection, the luciferase activity was measured in accordance with the instructions provided by the manufacturer. Assays were performed twice in triplicate. Data are means and s.d. for six determinations. **(d)** Immunoblot analysis. Flag-tagged p62 and its mutants defective in interacting with Keap1 were overproduced in wild-type and *p62*$^{-/-}$ primary mouse hepatocytes by the adenovirus system. At 48 h after infection, total cell lysates and nuclear fractions were prepared and subjected to immunoblot analysis with the antibodies specified. The bands corresponding to Flag–p62, endogenous p62, Keap1, Nrf2, Nqo1, actin and Lamin B are shown. Data are representative of three independent experiments. Uncropped images of blots are shown in Supplementary Information, Fig. S11. **(e)** Quantification of mRNA levels of the detoxification enzymes Nqo1, Gstm1 and Cyp2a5 in hepatocytes overexpressing Flag–p62 and its mutants. Total RNAs were prepared from non-infected or infected hepatocytes and reverse transcribed into their respective cDNAs, which were used as templates in real-time PCR analysis. Values were normalized to the amount of each mRNA in the non-infected hepatocytes. The experiments were performed three times. Data are means ± s.d. for three experiments.

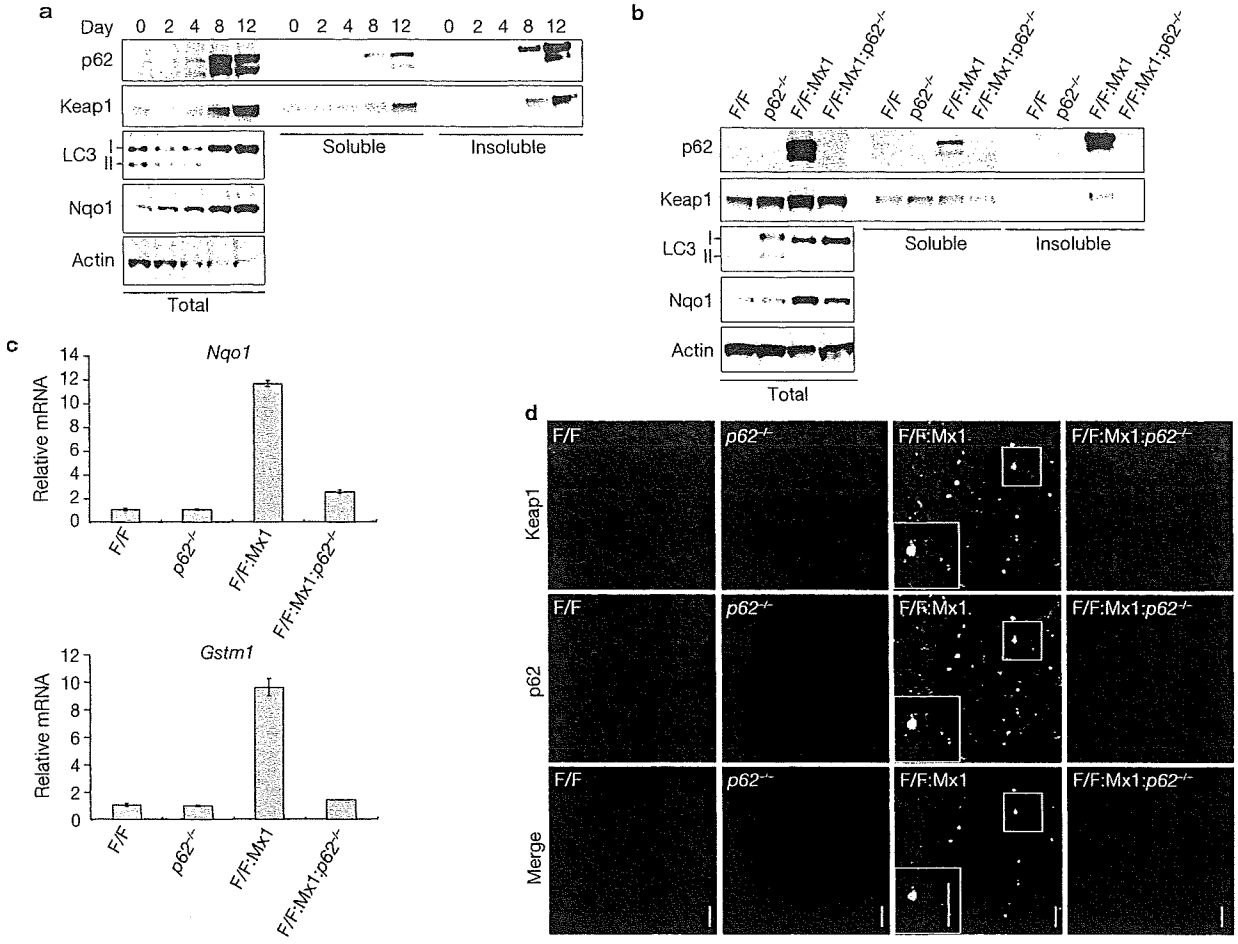


**Figure 4** Formation of p62-positive and Keap1-positive inclusions in autophagy-deficient hepatocytes. (**a**) Insolubilization of Keap1 in *Atg7*-deficient hepatocytes. Liver homogenates from *Atg7*$^{F/F}$:Mx1 mice on various days after injection of poly(I)•poly(C) were separated into detergent-soluble and detergent-insoluble fractions with 0.5% Triton X-100. Each fraction was subjected to SDS–PAGE and analysed by immunoblotting with the indicated antibodies. The data displayed are representative of three separate experiments. (**b**) Immunoblot analysis of *Atg7*-deficient (*Atg7*$^{F/F}$:Mx1; *Atg7*$^{F/F}$ shown here as F/F) and *Atg7 p62*-deficient (*Atg7*$^{F/F}$:Mx1:*p62*$^{-/-}$) livers. Liver homogenates from mice of the stated genotypes at 12 days after injection of poly(I)•poly(C) were separated into detergent-soluble and detergent-insoluble fractions. Each fraction was subjected to SDS–PAGE and analysed by immunoblotting with the indicated antibodies. *Atg7*$^{F/F}$ mice[2] in which Atg7 is efficiently expressed at a level similar to that in the wild-type mice were used as control. Data shown are representative of three separate experiments. Uncropped images of blots are shown in Supplementary Information, Fig. S11. (**c**) Quantitative real-time PCR analyses of Nqo1 and Gstm1 in mouse livers. Total RNAs were prepared from livers of the indicated genotypes at 12 days after injection of poly(I)•poly(C). Values were normalized to the amount of mRNA in *Atg7*$^{F/F}$ liver. Data are means ± s.d. for three experiments. (**d**) Immunofluorescence analysis of the cellular localization of p62 and Keap1. Liver sections from mice of the indicated genotypes at 28 days after injection of poly(I)•poly(C) were immunostained with anti-Keap1 (top) and anti-p62 (middle) antibodies. Bottom: merged images of Keap1 (green) and p62 (red). Each inset in the *Atg7*-deficient liver panels is a magnified image of the boxed region. Scale bars, 20 μm.

Information, Fig. S1), suggesting the existence of p62-dependent regulation of Nrf2.

To explore cellular regulation by p62, we used a proteomic approach[34] to screen for proteins that interact with p62, by using HEK293T cells expressing tagged p62 protein. Keap1 was identified as a p62-interacting protein (data not shown). In an independent experiment with RL34 cells expressing tagged Keap1 protein, we isolated p62 as a Keap1-associating protein (data not shown). Keap1 is a substrate adaptor protein for Cullin-3-type ubiquitin E3 ligase. Keap1 possesses four domains: the Broad complex, Tramtrack, and Bric-a-Brac (BTB, amino-acid residues 61–179); the intervening region (IVR, residues 180–314); the double glycine repeat or kelch repeat (DGR, residues 315–598); and the carboxy-terminal region (CTR, residues 599–624)[24–27] (Fig. 1a). The DGR and CTR domains are collectively called the DC domain. The BTB domain serves to dimerize Keap1, enabling ubiquitin conjugation onto specific lysine residues located within the Neh2 domain of Nrf2 (refs 35, 36). The IVR domain interacts with Cullin 3 to promote Nrf2 ubiquitylation[26], whereas the DC domain physically interacts with the Neh2 domain of Nrf2 (refs 36 37). To specify the regions of Keap1 essential for its interaction with p62, we performed an immunoprecipitation assay. Whereas Keap1 C-terminal deletion mutants (ΔDGR and ΔCTR) did not interact with either endogenous p62 or Nrf2, Keap1 amino-terminal deletion mutants (ΔNTR, ΔBTB and ΔIVR) interacted with both endogenous p62 and Nrf2, although with weaker affinities than wild-type Keap1 (Fig. 1a). The Keap1-DC domain, but not the DGR domain, bound to both p62 and Nrf2 (Fig. 1a). The CTR domain contributes to the structural fold of Keap1-DC, which is required for interaction with Nrf2 (ref. 38). These results therefore suggest that the six-bladed β-propeller structure of Keap1 is essential for its molecular recognition of p62, as is the case for Nrf2.

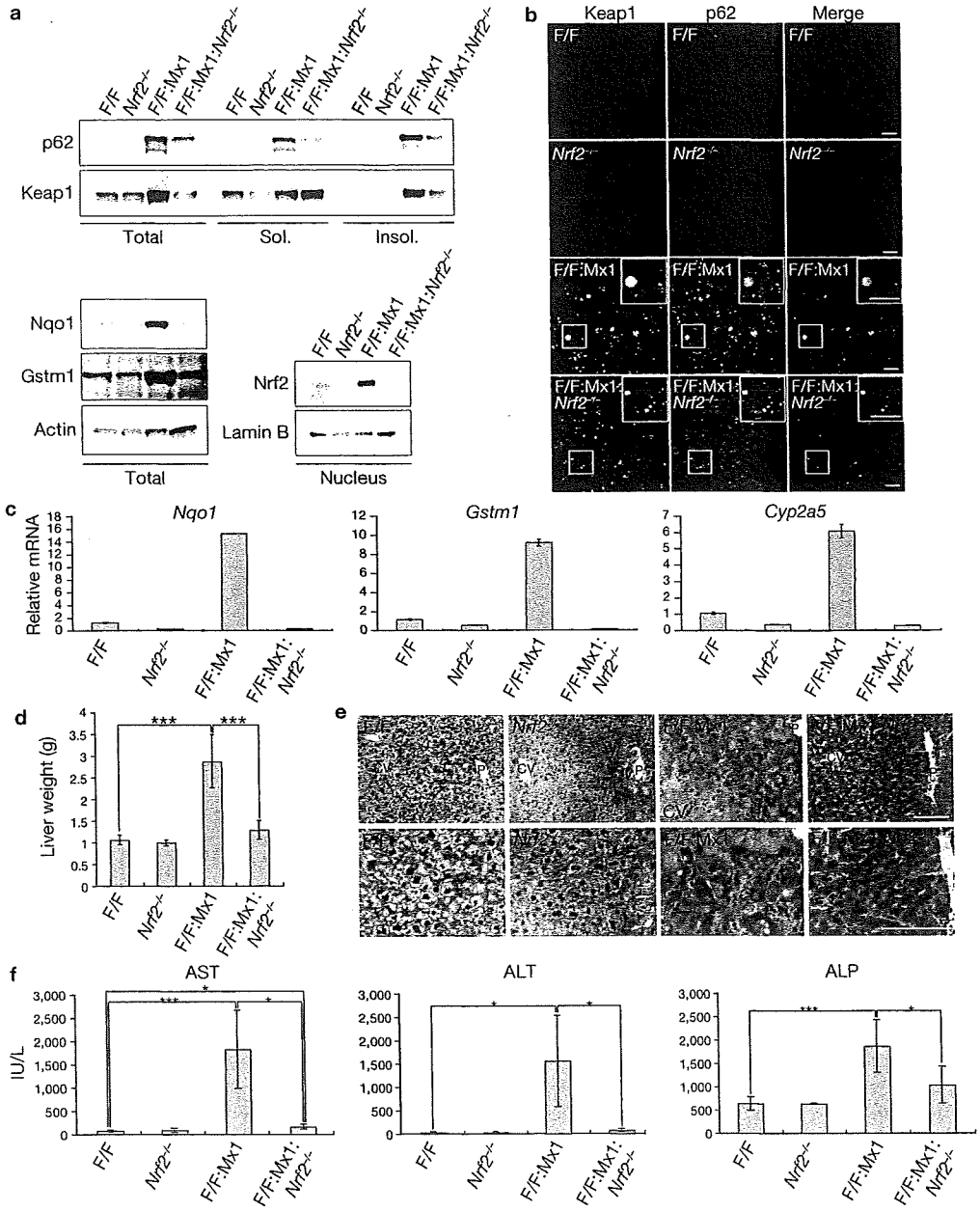


**Figure 5** Amelioration of liver dysfunction in autophagy-deficient mice by the additional loss of *Nrf2*. (**a**) Immunoblotting of *Atg7*-deficient (*Atg7*$^{F/F}$:Mx1; *Atg7*$^{F/F}$ shown here as F/F) and *Atg7 Nrf2*-deficient (*Atg7*$^{F/F}$:Mx1:*Nrf2*$^{-/-}$) livers. Liver homogenates from mice of the assigned genotypes at 28 days after injection of poly(I)•poly(C) were separated into detergent-soluble and detergent-insoluble fractions. Total, soluble and insoluble fractions were subjected to SDS–PAGE and analysed by immunoblotting with the indicated antibodies (top section). Total lysates were subjected to SDS–PAGE and analysed by immunoblotting with antibodies against Nqo1, Gstm1 and actin (bottom left section). Nuclear fractions were prepared from the livers of the indicated genotypes at 28 days after injection of poly(I)•poly(C), subjected to SDS–PAGE and analysed by immunoblotting with antibodies against Nrf2 and Lamin B (as control) (bottom right section). Data were obtained from three independent experiments. Uncropped images of blots are shown in Supplementary Information, Fig. S11. (**b**) Immunofluorescence analysis of the cellular localization of p62 and Keap1. Liver sections from mice of the indicated genotypes at 28 days after injection of poly(I)•poly(C) were immunostained with anti-Keap1 (left) and anti-p62 (middle) antibodies. Right: merged images of Keap1 (green) and p62 (red). Each inset in the *Atg7*-deficient and *Atg7 Nrf2*-deficient liver panels is a magnified image of the boxed region. Scale bars, 20 μm. (**c**) Quantitative real-time PCR analyses of Nqo1, Gstm1 and Cy2a5 in mouse livers. Total RNAs were prepared from livers of the indicated genotypes at 28 days after injection of poly(I)•poly(C). Values were normalized to the amount of mRNA in the *Atg7*$^{F/F}$ liver. Data are means ± s.d. for three experiments. (**d**) Liver weight. The weights of the mouse livers of the different genotypes shown at 28 days after injection of poly(I)•poly(C) were measured. Data are means ± s.d. for five mice from each group. Three asterisks, $P < 0.001$ (Student's *t*-test). (**e**) Histological analysis of the mouse liver of the indicated genotypes. At 28 days after injection of poly(I)•poly(C), the livers were processed for haematoxylin/eosin staining. Higher-magnification views are shown in the bottom panels. CV, central vein; P, portal vein. Scale bars, 100 μm. (**f**) Liver function tests of the mice used in **d**. The serum levels of aspartate aminotransferase (AST), alanine aminotransferase (ALT) and alkaline phosphatase (ALP) were measured. (IU/L, international unit per liter). Data are means ± s.d. for seven mice from each group. Asterisk, $P < 0.05$; three asterisks, $P < 0.001$.

p62 comprises an N-terminal region that includes Phox and Bem1p (PB1) (residues 20–102) and a zinc finger (residues 122–167), a central region containing an LC3-recognition sequence (LRS) (residues 337–343), and a C-terminal region encompassing a ubiquitin-associated domain (UBA) (residues 391–436)[14,15,39] (Fig. 1b). To determine which domain of p62 is required for its interaction with Keap1, we divided p62 into three regions and employed a pull-down assay with the Keap1-DC domain (Supplementary Information, Fig. S2). The Keap1-DC domain was clearly detected in pull-down products both with full-length p62 and with p62M7, the p62 mutant harbouring the central region (residues 168–391). However, deletion mutants p62M3 and p62M5 showed a marked decrease in binding to the Keap1-DC domain (Supplementary Information, Fig. S2). To delineate the interaction domain more precisely, we prepared a deletion series of p62M7 (M71–M83) and performed the pull-down assay (Fig. 1b; Supplementary Information, Fig. S3a). These assays revealed that p62M83, covering residues 345–359, is essential and sufficient for the interaction between p62 and Keap1-DC (Supplementary Information, Fig. S3a). We therefore named residues 346–359 in p62M83 the Keap1-interacting region (KIR). KIR is located close to the C terminus of the LRS and is conserved across species (Fig. 1c). To further verify the Keap1–p62 interaction *in vivo*, we performed an immunoprecipitation assay. In primary mouse hepatocytes and HEK293T cells, endogenous Keap1 co-immunoprecipitated with wild-type Flag-tagged p62 and a mutant defective in oligomerization (p62 K7AD69A)[40], but failed to co-immunoprecipitate with KIR-deleted Flag–p62 (p62 ΔKIR) (Fig. 1d). The interaction between endogenous p62 and Keap1 was also verified (Fig. 1e).

## Crystal structure of Keap1-DC in complex with p62-KIR

To delineate how Keap1 interacts with p62-KIR, we determined the crystal structure of Keap1-DC (residues 309–624) in complex with the p62-KIR peptide covering residues 346–359 at a resolution of 2.8 Å. Keap1-DC forms a six-bladed β-propeller structure with pseudo six-fold symmetry[37,38]. The KIR peptide binds to the bottom side of the β-propeller structure (Fig. 2a, b). A simulated-annealing $F_o - F_c$ omit map clearly indicated the electron density in the peptide bound region, in which 8 residues (V348 to L355) out of 14 were visible in p62-KIR, except for the L355 side chain (Fig. 2c).

Nrf2 is turned over rapidly through proteasomal degradation[24–27]. We previously identified the DLG and ETGE binding motifs present in the Neh2 domain of Nrf2, and these two motifs bind individually to the same binding pocket located at the bottom surface of Keap1 (refs 37, 38). One Nrf2 molecule binds to the Keap1 homodimer or to two Keap1 molecules. Because the two-site binding facilitates the ubiquitylation of lysine residues located between the DLG and ETGE motifs, the two-site substrate recognition mechanism is crucial for the rapid ubiquitylation of Nrf2 (refs 37, 38). Hydrogen-bond analysis revealed that the interactions between the Keap1-DC domain and p62-KIR (Fig. 2d, left) heavily overlap with the interactions between the Keap1-DC domain and Nrf2-ETGE (Fig. 2d, right). Eight amino-acid residues of Keap1-DC (Y334, S363, R380, N382, R415, Q530, S555 and S602) form hydrogen bonds with p62-KIR. These eight residues and two additional Keap1 residues (R483 and S508) are involved in Keap1 recognition of Nrf2-ETGE. These data strongly support the notion that p62-KIR binds to Keap1 in a manner very similar to that of the Nrf2-ETGE and Nrf2-DLG motifs[37,38].

The complex structure of Keap1-DC and p62-KIR showed that, of the eight amino-acid residues of the KIR domain, five residues (P350, S351, T352, E354 and L355) are involved in the interaction with Keap1 (Fig. 2d, left). To further verify this interaction biochemically, point mutations were created in the amino-acid residues of KIR in the mutant construct p62M80 by alanine replacement (Supplementary Information, Fig. S3a). A pull-down assay revealed that formation of the Keap1-DC–p62M80 complex was significantly decreased in the D349A, P350A, T352A, G353A and E354A mutants (Supplementary Information, Fig. S3a). Consistent with this experiment, immunoprecipitation analysis also revealed that these mutants showed a marked decrease in binding to Keap1 (Supplementary Information, Fig. S3b). The S351A mutation did not affect binding to Keap1 in either experiment, in spite of the direct interaction between S351 and Keap1 (Fig. 2d, left). The D349A mutation significantly inhibited the interaction with Keap1 (Supplementary Information, Fig. S3b), even though D349 does not interact directly with Keap1 (Fig. 2d, left). Residue D349 is involved in intra-peptide hydrogen bonding with S351 and T352, which stabilizes the type I β-turn in p62-KIR (Fig. 2e); this seems to be critical for the interaction between Keap1-DC and p62-KIR.

Because the tertiary structure of the complex indicates that p62-KIR associates with eight amino-acid residues in the basic surface of Keap1-DC, we introduced mutations in the residues of Keap1-DC (Y334, S363, R380, N382, R415, S508, Q530, S555 and S602) that are critical in the interaction with the KIR domain, and executed a GST pull-down assay (Supplementary Information, Fig. S3c). All except one of these GST–Keap1-DC mutants were markedly impaired in their ability to pull down maltose-binding protein (MBP)–p62M80 (Supplementary Information, Fig. S3c); the exception was R483A, which is not involved in the interaction with KIR (Fig. 2d). Further immunoprecipitation analysis confirmed that these residues in Keap1 are essential for efficient interaction with endogenous p62 and Nrf2 (Supplementary Information, Fig. S3d). These biochemical results are in good agreement with the crystal structure analysis.

## Competitive inhibition of the Nrf2–Keap1 pathway by p62

Previous structural and kinetics studies demonstrated that the ETGE motif has a high affinity but the DLG motif has a low affinity for the same basic surface of Keap1 ($K_{a,ETGE} = (1.90 \pm 0.40) \times 10^8\ M^{-1}$, compared with $K_{a,DLG} = (1.00 \pm 0.00) \times 10^6\ M^{-1}$) (ref. 41). If the affinity of the p62 KIR domain for the basic surface in Keap1 were higher than or comparable to that of the ETGE or DLG motif, p62 might serve as an endogenous protein inducer of Nrf2 target genes by competitive binding inhibition of the Nrf2–Keap1 complex. It was therefore important to determine the binding-dissociation constant of Keap1–p62. Assessment of the binding energy by isothermal titration calorimetry (ITC) showed that the affinity of p62M7 (residues 168–391) for Keap1-DC ($K_a = (5.4 \pm 0.3) \times 10^5\ M^{-1}$) was similar to that of the DLG motif (Fig. 3a) and that, unlike with Nrf2, the binding stoichiometry was 1:1. This result suggests that overproduction of p62 counteracts the interaction between Nrf2-DLG and Keap1, but not that between Nrf2-ETGE and Keap1. In support of this notion, whereas the amounts of p62 forming a complex with Flag–Keap1 increased in proportion to the p62 expression level, the levels of Nrf2 interacting with Keap1 were hardly affected by overexpression of p62 (Fig. 3b). Meanwhile, p62 overproduction led to a marked decrease in Nrf2 ubiquitylation (see Supplementary Information, Fig. S4) and consequent Nrf2 stabilization (see Fig. 3d), suggesting that p62 inhibits Nrf2-DLG, but not Nrf2-ETGE, from interacting with Keap1.

So far, structural and kinetic analyses have strongly argued that p62 competitively inhibits the Keap1–Nrf2 interaction, leading to

the stabilization of Nrf2 and the expression of cytoprotective genes. To verify this concept further, we performed luciferase assays with a reporter plasmid harbouring the canonical Nrf2 recognition motif referred to as the ARE (antioxidant-responsive element). The transactivation activity of Nrf2 was suppressed by simultaneous expression of Keap1 (Fig. 3c, lanes 2 and 3), but this repression by Keap1 was inhibited by overexpression of p62 (Fig. 3c, lane 4). Mutants of p62 defective in interaction with Keap1 failed to counteract the repression of Nrf2 activity by Keap1 (Fig. 3c, lanes 5–10). Even in the absence of Keap1 transfection, p62 overexpression activated reporter gene expression (Fig. 3c, lane 11), perhaps by targeting the interaction of endogenous Keap1 with Nrf2; however, p62 mutants did not show this activity (Fig. 3c, lanes 12–17). This antagonistic effect of p62 to Keap1 seems to be independent of the self-oligomerization ability of p62 because the oligomerization-defective mutant p62 K7AD69A similarly counteracted the repression by Keap1 (Supplementary Information, Fig. S5a).

To examine whether p62 overexpression reinforces Nrf2 stability, we infected wild-type and *p62*$^{-/-}$ mouse primary hepatocytes with adenovirus Flag-tagged wild-type p62 and p62 mutants (ΔKIR, T352A and E354A) severely attenuated in their interactions with Keap1 (see Fig. 1d for ΔKIR; see Supplementary Information, Fig. S3a, b, for T352A and E354A). In both wild-type and mutant hepatocytes, overproduction of Flag–p62, but not of the mutants, triggered an increase in both total Nrf2 (Fig. 3d, upper panel) and the level of Nrf2 in the nuclear fractions (Fig. 3d, lower panel; Supplementary Information, Fig. S6). Because overproduction of Flag–p62, but not of the mutants, in primary mouse hepatocytes significantly inhibited Nrf2 ubiquitylation (Supplementary Information, Fig. S4), the Nrf2 stabilization can be attributed to Nrf2 being outcompeted by p62 for Keap1 binding. Consistent with this conclusion, the expression of Nrf2 target genes, such as *Nqo1*, *Gstm1* and *Cyp2a5*, was induced by the expression of Flag–p62, but not by expression of the mutants deficient in interaction with Keap1 (Fig. 3d, e; Supplementary Information, Fig. S6). In contrast, another p62 mutant (K7AD69A), which was defective in self-oligomerization but able to interact with Keap1 (see Fig. 1d) activated Nrf2 target genes to a modest but significant extent (Supplementary Information, Fig. S5b, c).

## Keap1 is sequestered in inclusion bodies in a p62-dependent manner

The next series of experiments served to clarify whether the Nrf2–Keap1 interaction is affected by the intracellular accumulation of p62 or p62-positive and ubiquitin-positive inclusion bodies, which is known to occur in autophagy-deficient liver[16]. These studies were conducted in *Atg7*$^{F/F}$:Mx1 mice in which *Atg7* can be depleted in the liver by intraperitoneal injection of polyinosinic acid•polycytidylic acid (poly(I)•poly(C))[2]. Consistent with our previous work[16], immunoblot analysis revealed that p62 started to accumulate at day 4, was abundant in both the detergent-soluble and insoluble fractions at day 8 and further increased in both fractions at day 12 after injection of poly(I)•poly(C) (Fig. 4a). This pattern correlated well with the decrease in conversion of LC3-I to LC3-II, which signifies defective autophagosome formation[42] (Fig. 4a). On accumulation of p62, Keap1 was detected abundantly, especially in the detergent-insoluble fraction (Fig. 4a). The quantity of Nqo1 also increased gradually in *Atg7*-deficient livers (Fig. 4a), suggesting that Keap1 was inactivated by the loss of autophagy.

To determine whether the accumulation of Keap1 in the insoluble fraction of autophagy-deficient livers depends on the presence of p62, we used *Atg7*:*p62*-double-knockout mice (*Atg7*$^{F/F}$:Mx1:*p62*$^{-/-}$ or *Atg7 p62* DKO)[16]. The concurrent loss of *Atg7* and *p62* in the liver significantly suppressed the accumulation of Keap1 in the insoluble fraction that was observed in *Atg7*-deficient livers (Fig. 4b). This indicates that Keap1 is inactivated in a p62-dependent manner. Indeed, the high mRNA and protein levels of Nrf2 target genes in *Atg7*-deficient livers returned to almost normal levels after the additional loss of p62 (Fig. 4b, c). Immunofluorescence microscopy showed that the numerous Keap1-positive inclusions of various sizes seen in *Atg7*-deficient hepatocytes were absent from *Atg7 p62*-DKO hepatocytes (Fig. 4d). Double immunofluorescence microscopy showed that most of the Keap1-containing inclusions observed in *Atg7*-deficient hepatocytes were also positive for p62 (Fig. 4d). Taken together, these results indicate that under conditions of suppressed autophagy, a significant population of Keap1 is trapped by the excessive upsurge in p62, leading to sequestration of Keap1 into p62-positive and ubiquitin-positive inclusions.

## Liver injury in autophagy-deficient mice is alleviated by loss of *Nrf2*

Although the excessive build-up of p62 seems to be the main cause of the pathogenic changes seen in the livers of autophagy-deficient mice, the molecular events involved in the pathogenic onset are still unknown. The data described so far suggest that p62-dependent regulation of the Nrf2–Keap1 pathway is involved in the pathological changes found in autophagy-deficient mice. To address this point, we crossed *Atg7*$^{F/F}$:Mx1 mice with *Nrf2*$^{-/-}$ mice[21] to produce *Atg7*:*Nrf2*-double-knockout mice (*Atg7*$^{F/F}$:Mx1:*Nrf2*$^{-/-}$ or *Atg7 Nrf2* DKO). Immunoblot analysis revealed that although the amount of p62 in *Atg7 Nrf2*-DKO livers was lower than that in *Atg7*-deficient livers, it was markedly higher than in control and *Nrf2*-knockout mouse livers (Fig. 5a). About half of the p62 in *Atg7 Nrf2*-DKO livers and *Atg7*-deficient livers was recovered in the insoluble fraction (Fig. 5a). The lower p62 level in *Atg7 Nrf2*-DKO mouse livers might be attributable, at least in part, to the loss of Nrf2 regulation for *p62* gene transcription[43]. Keap1 was also fractionated into the insoluble fraction in *Atg7*-deficient and *Atg7 Nrf2*-DKO mouse livers in proportion to the amount of insoluble p62 (Fig. 5a). The Keap1-positive aggregates detected in *Atg7*-deficient hepatocytes were also found in *Atg7 Nrf2*-DKO hepatocytes, although the aggregates were smaller and were almost completely co-localized with p62 (Fig. 5b). Electron microscopy showed accumulation of organelles and inclusion bodies in *Atg7 Nrf2*-DKO hepatocytes, similar to that observed in *Atg7*-deficient hepatocytes (Supplementary Information, Fig. S7). However, in contrast to *Atg7*-deficient livers, the induction of antioxidant proteins and detoxifying enzymes was completely abrogated in *Atg7 Nrf2*-DKO livers (Fig. 5a, c), confirming the Nrf2-dependent transcriptional induction of cytoprotective enzymes in autophagy-deficient livers.

We further examined the liver damage in these mice. Increased liver weight (Fig. 5d), disorganization of lobular structures (Fig. 5e, upper panels), hepatocytic hypertrophy (Fig. 5e, lower panels), an increased proportion of infiltrating cells (data not shown), and higher serum levels of aspartate aminotransferase, alanine aminotransferase and alkaline phosphatase (Fig. 5f) were observed in *Atg7*-deficient livers[2]; these were significantly suppressed by the additional loss of *Nrf2*. These results strongly suggest that persistent activation of Nrf2 in autophagy-deficient conditions may be one of the main causes of liver injury.

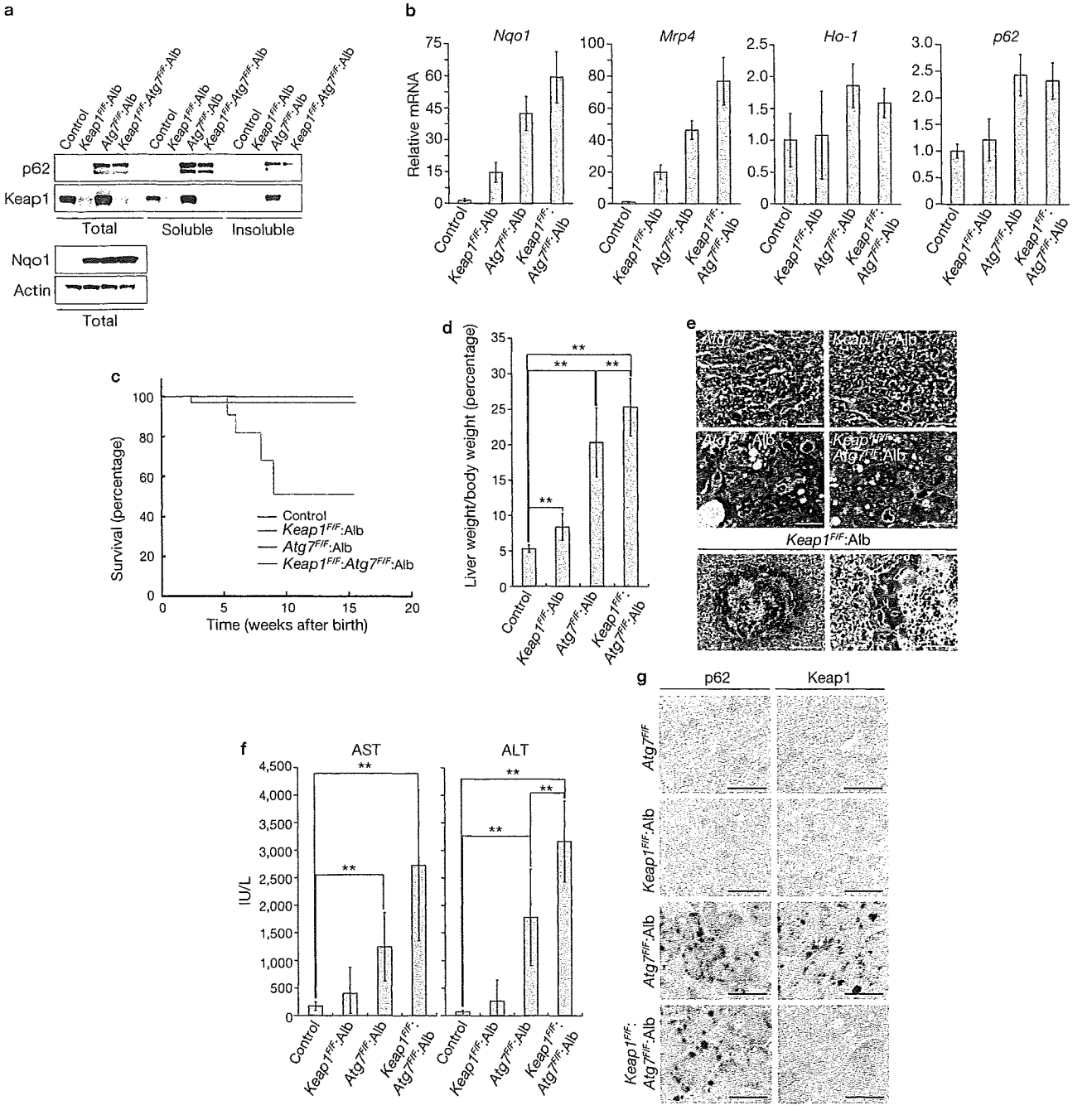


**Figure 6** Exacerbation of liver dysfunction in autophagy-deficient mice by the additional loss of *Keap1*. (**a**) Immunoblotting of *Keap1*-deficient (*Keap1*$^{F/F}$:Alb) and *Keap1 Atg7*-deficient (*Keap1*$^{F/F}$:*Atg7*$^{F/F}$:Alb) livers. Liver homogenates from 8-week-old mice of these genotypes were separated into detergent-soluble and detergent-insoluble fractions. Total, soluble and insoluble fractions were subjected to SDS–PAGE and analysed by immunoblotting with the indicated antibodies (top section). Total lysates were subjected to SDS–PAGE and analysed by immunoblotting with antibodies against Nqo1 and actin (bottom section). Data were obtained from three independent experiments. Uncropped images of blots are shown in Supplementary Information, Fig. S11. (**b**) Quantitative real-time PCR analyses of Nqo1, Mrp4, p62 and Ho-1 in mouse livers. Total RNAs were prepared from livers of 9-week-old indicated genotypes. Values were normalized to the amount of mRNA in the *Atg7*$^{F/F}$ liver (control). Data are means ± s.d. for three experiments. (**c**) Kaplan–Meier curves of survival of *Atg7*$^{F/F}$:Alb and *Keap1*$^{F/F}$:*Atg7*$^{F/F}$:Alb mice. The survival analysis of control ($n = 33$), *Keap1*$^{F/F}$:Alb ($n = 15$), *Atg7*$^{F/F}$:Alb ($n = 12$) and *Keap1*$^{F/F}$:*Atg7*$^{F/F}$:Alb mice ($n = 14$) was based on a 16-week follow-up period. (**d**) Liver weight relative to body weight was measured for the different genotypes. Data are means ± s.d. for *Atg7*$^{F/F}$ (control) ($n = 24$), *Keap1*$^{F/F}$:Alb ($n = 13$), *Atg7*$^{F/F}$:Alb ($n = 9$) and *Keap1*$^{F/F}$:*Atg7*$^{F/F}$:Alb mice ($n = 7$). Two asterisks, $P < 0.01$ (Student's *t*-test). (**e**) Histological analysis of mouse liver of the indicated genotypes. The livers from 9-week-old mice were processed for haematoxylin/eosin staining. Scale bar, 50 μm (left bottom panel); 20 μm (other panels). (**f**) Liver function tests of the mice used in **d**. The serum levels of aspartate aminotransferase (AST) and alanine aminotransferase (ALT) were measured. Data are means ± s.d. for *Atg7*$^{F/F}$ (control) ($n = 24$), *Keap1*$^{F/F}$:Alb ($n = 13$), *Atg7*$^{F/F}$:Alb ($n = 9$) and *Keap1*$^{F/F}$:*Atg7*$^{F/F}$:Alb mice ($n = 7$). Two asterisks, $P < 0.01$. (**g**) Immunohistochemical analysis of cellular localization of p62 and Keap1. Paraffin sections of the liver from 9-week-old mice of the indicated genotypes were immunolabelled with anti-p62 (left) and anti-Keap1 (right) antibodies. Scale bars, 20 μm.

### Liver injury in autophagy-deficient mice is exacerbated by loss of *Keap1*

To consolidate the notion that persistent activation of Nrf2 accompanied by defective autophagy causes liver injury, we generated hepatocyte-specific *Keap1*:*Atg7*-double-knockout mice (*Keap1*$^{F/F}$:*Atg7*$^{F/F}$:Alb or *Keap1 Atg7* DKO) by crossing *Keap1*$^{F/F}$:Alb[44] with *Atg7*$^{F/F}$ mice. *Keap1*-deficient mouse livers showed hyper-activation of Nrf2 (Fig. 6a, b), mild hepatomegaly (Fig. 6d) and occasional focal necrotic cell death (Fig. 6e, bottom panels), indicating that persistent activation of Nrf2 provokes cytotoxicity. Both the mRNA and protein levels of typical Nrf2 target genes in the *Keap1 Atg7*-DKO livers were significantly higher than those in single *Atg7*-knockout mouse livers (Fig. 6a, b), demonstrating that the loss of *Keap1* additively activates Nrf2 in autophagy-deficient livers. However, this additive effect was observed in only some Nrf2 target genes, such as *Nqo1* and *Mrp4*, but not in the other target genes, including those encoding p62 and haem oxygenase-1 (Ho-1) (Fig. 6a, b). Thus, transactivation by Nrf2 of certain Nrf2 target genes might be saturated in *Atg7*-deficient livers, so that levels of p62 and p62-positive aggregates in the *Keap1 Atg7*-DKO livers seemed to be similar to those in *Atg7*-deficient livers (Fig. 6a, g).

Although *Keap1 Atg7*-DKO mice were born at a Mendelian frequency, the survival rate of these mice diminished markedly 6 weeks after birth (Fig. 6c). We observed growth retardation at about 4 weeks (data not shown). Histological analysis showed pathological changes in DKO liver that were similar to those observed in *Atg7*-deficient liver: hepatocytic swellings and/or necrotic changes, appearance of acidophilic bodies, and cellular infiltration (Fig. 6e). The DKO mice showed increased liver weight (relative to body weight; Fig. 6d) and a high level of serum alanine aminotransferase (Fig. 6f) compared with *Atg7*-single-knockout mice. These results further support our conclusion that autophagy deficiency provokes deregulation of the Nrf2–Keap1 system and that constitutive activation of Nrf2 leads to hepatotoxicity.

## DISCUSSION

In this study we have demonstrated that p62 serves as an endogenous protein inducer of Nrf2. We previously deciphered the unique association mechanism of Nrf2 and Keap1 in which two Keap1 molecules interact with one Nrf2 molecule through its DLG and ETGE motifs. This two-site binding facilitates the ubiquitylation and degradation of Nrf2 (refs 37, 38). This mechanism has been verified by the finding that, in cases of human lung cancer, somatic mutations in Nrf2 are located exclusively in the DLG and ETGE motifs[45]. We proposed the 'hinge and latch' model as the stress-sensing mechanism, by which the weak-affinity DLG motif acts as a latch for turning the ubiquitylation of Nrf2 on or off (refs 37, 41). Here we found that, on perturbation of autophagy, p62 accumulates and activates Nrf2 by competing with Nrf2 for its binding to Keap1. The following observations are significant: first, through its KIR motif, p62 interacts directly with Keap1; second, the binding mode of KIR is similar to that of Nrf2-ETGE or Nrf2-DLG, where it binds to the basic surface pocket at the bottom of Keap1; and third, p62-KIR binds to Keap1 with an affinity similar to that of Nrf2-DLG but much weaker than that of Nrf2-ETGE. It therefore seems most plausible that the KIR motif interferes directly with the binding of the DLG motif to Keap1. These results support our argument that the 'hinge and latch' mechanism actually operates *in vivo* (see the model in Supplementary Information, Fig. S10).

Our present study demonstrates that the pathological changes observed in autophagy-defective livers are due, at least in part, to persistent activation of Nrf2 by the excess accumulation of p62. This was an unexpected result because most Nrf2-dependent gene products retain cytoprotective function[31]. To verify this finding further, we performed a microarray analysis in *Atg7*-knockout and *Atg7 Nrf2*-DKO mouse livers. The analysis showed that more than 100 genes were activated in an Nrf2-dependent manner in autophagy-deficient livers, with a range of induction from 2-fold to as much as 100-fold (data not shown, and Fig. 5c). Furthermore, our comprehensive proteomics analysis reported previously[46] showed that the Nrf2 target gene products, such as Gst-m1 and Gst-p1, were prominent proteins in autophagy-deficient liver. Surprisingly, Gst-m1 constituted 7.69 ± 1.25% of the cytosolic proteins in *Atg7*-deficient livers (Supplementary Information, Fig. S8). Thus, the autophagy-deficient liver shows an abnormal accumulation of various Nrf2 target proteins. Because loss of *Keap1* in mouse hepatocytes resulted in only mild liver abnormality (Fig. 6d, e), the phenotypes detected in *Atg7*-deficient livers cannot be attributed solely to Nrf2 activation by loss of *Keap1*. It is therefore conceivable that the additional loss of autophagy greatly affects the development of liver abnormality. In other words, the collapse of the balance between the synthesis of cellular proteins (Nrf2-dependent robust protein synthesis) and their degradation (global turnover of cytoplasmic proteins through autophagy) could result in the appearance of destructive phenotypes (that is, hepatocytic hypertrophy due to the increased cellular protein volume followed by hepatomegaly and liver injury). In support of this conclusion, hepatocyte-specific *Keap1 Atg7*-DKO mice showing high-level Nrf2 activity exhibited more severe hepatomegaly and liver injury than the single *Atg7*-deficient mice (Fig. 6c–f).

It has been reported that p62 accumulation in growing cell lines leads to a decrease in the ubiquitin–proteasomal (UPS) flux[47], implying that the cytotoxicity of p62 operates through inhibition of the UPS flux. However, overproduction of p62 did not induce inhibition of the UPS flux in primary culture hepatocytes (data not shown), suggesting that p62 accumulation is not cytotoxic towards quiescent cells. In fact, forced overexpression of p62 in primary culture hepatocytes lacking both *Atg7* and *p62* activated the expression of Nrf2 target genes but did not induce cell death (Supplementary Information, Fig. S9). We surmise that the hepatic injury caused by the *Atg7* deficiency is not attributable to cell-autonomous failure but rather to disintegration of the liver tissue as a result of hypertrophy of the hepatocytes. Indeed, both narrowing of sinusoidal capillaries and abnormal morphology of bile canaliculi were evident in *Atg7*-deficient liver (Figs 5e and 6e), suggesting that severe cholestasis and/or haemostasis might be the main causes of the liver injury.

Accumulation of p62, and/or p62-positive inclusions, has been reported in human liver diseases such as hepatocellular carcinoma, alcoholic hepatitis and $\alpha_1$-antitrypsin deficiency[20]. We propose that in such pathological conditions, the high levels of p62 associated with the suppression of autophagy might result in activation of Nrf2. Further analysis is needed to clarify the regulation or dysregulation of the Nrf2–Keap1 pathway in these human diseases. □

## METHODS

Methods and any associated references are available in the online version of the paper at http://www.nature.com/naturecellbiology/

*Note: Supplementary Information is available on the Nature Cell Biology website.*

ACKNOWLEDGEMENTS

We thank T. Kouno and K. Endo (Tokyo Metropolitan Institute of Medical Science) for technical assistance, and the beamline staff at NW12 of PF-AR (Tsukuba, Japan) for technical help in data collection. We also thank A. Yamada, K. Kanno

and A. Yabashi (Fukushima Medical University School of Medicine) for their help in histological studies; J. Yanagisawa (Tsukuba University) and Y. Saeki (Tokyo Metropolitan Institute of Medical Science) for mass spectrometric analyses; Y. Kawatani (Tohoku University) for technical assistance in microarray analyses; and R. Kopito and B. E. Riley (Stanford University) and T. Mizushima and T. Kumanomidou (Nagoya University) for helpful discussion. *p62*-knockout mice were provided by T. Ishii (Tsukuba University). The Biomedical Research Core of Tohoku University Graduate School of Medicine provided DRI-CHEM 7000V (Fuji Film Corp.). This work was supported by grants from the Japan Science and Technology Agency (M.K.), the Ministry of Education, Science and Culture of Japan (M.K., K.T. and M.Y.) and the Targeted Proteins Research Program (H.K., K.T. and M.Y.).

## AUTHOR CONTRIBUTIONS

M.K., K.T., I.U. and A.S. performed most of the experiments that characterized the knockout mice. I.U., Y.-S.S., Y.I. and A.K. performed the biochemical and cell biological experiments. Y.N. carried out microarray analyses. S.-i.I and T.N. performed mass spectrometric analyses. S.W. performed the histological and microscopic analyses. Structural and kinetics analyses were completed by H.K. and K.I.T. M.K., K.T. and M.Y. conceived the experiments. M.K., H.K., S.W., H.M., K.T. and M.Y. wrote the paper. E.K. and T.U. provided intellectual support. All authors discussed the results and commented on the manuscript.

## COMPETING FINANCIAL INTERESTS

The authors declare no competing financial interests.

Published online at http://www.nature.com/naturecellbiology
Reprints and permissions information is available online at http://npg.nature.com/reprintsandpermissions/

1. Mizushima, N., Levine, B., Cuervo, A. M. & Klionsky, D. J. Autophagy fights disease through cellular self-digestion. *Nature* **451,** 1069–1075 (2008).
2. Komatsu, M. *et al.* Impairment of starvation-induced and constitutive autophagy in Atg7-deficient mice. *J. Cell Biol.* **169,** 425–434 (2005).
3. Ebato, C. *et al.* Autophagy is important in islet homeostasis and compensatory increase of beta cell mass in response to high-fat diet. *Cell Metab.* **8,** 325–332 (2008).
4. Jung, H. S. *et al.* Loss of autophagy diminishes pancreatic beta cell mass and function with resultant hyperglycemia. *Cell Metab.* **8,** 318–324 (2008).
5. Nakai, A. *et al.* The role of autophagy in cardiomyocytes in the basal state and in response to hemodynamic stress. *Nature Med.* **13,** 619–624 (2007).
6. Komatsu, M. *et al.* Loss of autophagy in the central nervous system causes neurodegeneration in mice. *Nature* **441,** 880–884 (2006).
7. Hara, T. *et al.* Suppression of basal autophagy in neural cells causes neurodegenerative disease in mice. *Nature* **441,** 885–889 (2006).
8. Yorimitsu, T. & Klionsky, D. J. Autophagy: molecular machinery for self-eating. *Cell Death Differ.* **12** (Suppl. 2), 1542–1552 (2005).
9. Rubinsztein, D. C. The roles of intracellular protein-degradation pathways in neurodegeneration. *Nature* **443,** 780–786 (2006).
10. Platta, H. W. & Erdmann, R. Peroxisomal dynamics. *Trends Cell Biol.* **17,** 474–484 (2007).
11. Zhang, J. & Ney, P. A. Role of BNIP3 and NIX in cell death, autophagy, and mitophagy. *Cell Death Differ.* **16,** 939-946 (2009).
12. Levine, B. & Deretic, V. Unveiling the roles of autophagy in innate and adaptive immunity. *Nature Rev. Immunol.* **7,** 767–777 (2007).
13. Bjorkoy, G. *et al.* p62/SQSTM1 forms protein aggregates degraded by autophagy and has a protective effect on huntingtin-induced cell death. *J. Cell Biol.* **171,** 603–614 (2005).
14. Pankiv, S. *et al.* p62/SQSTM1 binds directly to Atg8/LC3 to facilitate degradation of ubiquitinated protein aggregates by autophagy. *J. Biol. Chem.* **282,** 24131–24145 (2007).
15. Ichimura, Y. *et al.* Structural basis for sorting mechanism of p62 in selective autophagy. *J. Biol. Chem.* **283,** 22847–22857 (2008).
16. Komatsu, M. *et al.* Homeostatic levels of p62 control cytoplasmic inclusion body formation in autophagy-deficient mice. *Cell* **131,** 1149–1163 (2007).
17. Nezis, I. P. *et al.* Ref(2)P, the *Drosophila melanogaster* homologue of mammalian p62, is required for the formation of protein aggregates in adult brain. *J. Cell Biol.* **180,** 1065–1071 (2008).
18. Kuusisto, E., Salminen, A. & Alafuzoff, I. Ubiquitin-binding protein p62 is present in neuronal and glial inclusions in human tauopathies and synucleinopathies. *Neuroreport* **12,** 2085–2090 (2001).
19. Stumptner, C., Fuchsbichler, A., Heid, H., Zatloukal, K. & Denk, H. Mallory body — a disease-associated type of sequestosome. *Hepatology* **35,** 1053–1062 (2002).
20. Zatloukal, K. *et al.* p62 Is a common component of cytoplasmic inclusions in protein aggregation diseases. *Am J Pathol* **160,** 255–263 (2002).
21. Itoh, K. *et al.* An Nrf2/small Maf heterodimer mediates the induction of phase II detoxifying enzyme genes through antioxidant response elements. *Biochem. Biophys. Res. Commun.* **236,** 313–322 (1997).
22. Itoh, K. *et al.* Keap1 represses nuclear activation of antioxidant responsive elements by Nrf2 through binding to the amino-terminal Neh2 domain. *Genes Dev.* **13,** 76–86 (1999).
23. Wakabayashi, N. *et al.* Keap1-null mutation leads to postnatal lethality due to constitutive Nrf2 activation. *Nature Genet.* **35,** 238–245 (2003).
24. Cullinan, S. B., Gordan, J. D., Jin, J., Harper, J. W. & Diehl, J. A. The Keap1-BTB protein is an adaptor that bridges Nrf2 to a Cul3-based E3 ligase: oxidative stress sensing by a Cul3-Keap1 ligase. *Mol. Cell. Biol.* **24,** 8477–8486 (2004).
25. Furukawa, M. & Xiong, Y. BTB protein Keap1 targets antioxidant transcription factor Nrf2 for ubiquitination by the Cullin 3-Roc1 ligase. *Mol. Cell. Biol.* **25,** 162–171 (2005).
26. Kobayashi, A. *et al.* Oxidative stress sensor Keap1 functions as an adaptor for Cul3-based E3 ligase to regulate proteasomal degradation of Nrf2. *Mol. Cell. Biol.* **24,** 7130–7139 (2004).
27. Zhang, D. D., Lo, S. C., Cross, J. V., Templeton, D. J. & Hannink, M. Keap1 is a redox-regulated substrate adaptor protein for a Cul3-dependent ubiquitin ligase complex. *Mol. Cell. Biol.* **24,** 10941–10953 (2004).
28. Dinkova-Kostova, A. T. *et al.* Direct evidence that sulfhydryl groups of Keap1 are the sensors regulating induction of phase 2 enzymes that protect against carcinogens and oxidants. *Proc. Natl Acad. Sci. USA* **99,** 11908–11913 (2002).
29. Wakabayashi, N. *et al.* Protection against electrophile and oxidant stress by induction of the phase 2 response: fate of cysteines of the Keap1 sensor modified by inducers. *Proc. Natl Acad. Sci. USA* **101,** 2040–2045 (2004).
30. Kobayashi, A. *et al.* Oxidative and electrophilic stresses activate Nrf2 through inhibition of ubiquitination activity of Keap1. *Mol. Cell. Biol.* **26,** 221–229 (2006).
31. Motohashi, H. & Yamamoto, M. Nrf2–Keap1 defines a physiologically important stress response mechanism. *Trends Mol. Med.* **10,** 549–557 (2004).
32. Holtzclaw, W. D., Dinkova-Kostova, A. T. & Talalay, P. Protection against electrophile and oxidative stress by induction of phase 2 genes: the quest for the elusive sensor that responds to inducers. *Adv. Enzyme Regul.* **44,** 335–367 (2004).
33. Kobayashi, M. & Yamamoto, M. Nrf2–Keap1 regulation of cellular defense mechanisms against electrophiles and reactive oxygen species. *Adv. Enzyme Regul.* **46,** 113–140 (2006).
34. Komatsu, M. *et al.* A novel protein-conjugating system for Ufm1, a ubiquitin-fold modifier. *EMBO J.* **23,** 1977–1986 (2004).
35. Zipper, L. M. & Mulcahy, R. T. The Keap1 BTB/POZ dimerization function is required to sequester Nrf2 in cytoplasm. *J. Biol. Chem.* **277,** 36544–36552 (2002).
36. McMahon, M., Thomas, N., Itoh, K., Yamamoto, M. & Hayes, J. D. Dimerization of substrate adaptors can facilitate cullin-mediated ubiquitylation of proteins by a 'tethering' mechanism: a two-site interaction model for the Nrf2–Keap1 complex. *J. Biol. Chem.* **281,** 24756–24768 (2006).
37. Tong, K. I. *et al.* Different electrostatic potentials define ETGE and DLG motifs as hinge and latch in oxidative stress response. *Mol. Cell. Biol.* **27,** 7511–7521 (2007).
38. Padmanabhan, B. *et al.* Structural basis for defects of Keap1 activity provoked by its point mutations in lung cancer. *Mol. Cell* **21,** 689–700 (2006).
39. Seibenhener, M. L., Geetha, T. & Wooten, M. W. Sequestosome 1/p62 — More than just a scaffold. *FEBS Lett.* **581,** 175–179 (2007).
40. Lamark, T. *et al.* Interaction codes within the family of mammalian Phox and Bem1p domain-containing proteins. *J. Biol. Chem.* **278,** 34568–34581 (2003).
41. Tong, K. I. *et al.* Keap1 recruits Neh2 through binding to ETGE and DLG motifs: characterization of the two-site molecular recognition model. *Mol. Cell. Biol.* **26,** 2887–2900 (2006).
42. Kabeya, Y. *et al.* LC3, a mammalian homologue of yeast Apg8p, is localized in autophagosome membranes after processing. *EMBO J.* **19,** 5720–5728 (2000).
43. Ishii, T. *et al.* Transcription factor Nrf2 coordinately regulates a group of oxidative stress-inducible genes in macrophages. *J. Biol. Chem.* **275,** 16023–16029 (2000).
44. Okawa, H. *et al.* Hepatocyte-specific deletion of the *keap1* gene activates Nrf2 and confers potent resistance against acute drug toxicity. *Biochem. Biophys. Res. Commun.* **339,** 79–88 (2006).
45. Shibata, T. *et al.* Cancer related mutations in NRF2 impair its recognition by Keap1-Cul3 E3 ligase and promote malignancy. *Proc. Natl Acad. Sci. USA* **105,** 13568–13573 (2008).
46. Matsumoto, N. *et al.* Comprehensive proteomics analysis of autophagy-deficient mouse liver. *Biochem. Biophys. Res. Commun.* **368,** 643–649 (2008).
47. Korolchuk, V. I., Mansilla, A., Menzies, F. M. & Rubinsztein, D. C. Autophagy inhibition compromises degradation of ubiquitin–proteasome pathway substrates. *Mol. Cell* **33,** 517–527 (2009).

Biochimica et Biophysica Acta 1793 (2009) 1496–1507

Contents lists available at ScienceDirect

Biochimica et Biophysica Acta

journal homepage: www.elsevier.com/locate/bbamcr

Review

# The cellular pathways of neuronal autophagy and their implication in neurodegenerative diseases

Zhenyu Yue [a,*], Lauren Friedman [a], Masaaki Komatsu [b], Keiji Tanaka [b]

[a] Department of Neurology and Neuroscience, Mount Sinai School of Medicine, New York, NY 10029, USA
[b] Laboratory of Frontier Science; Tokyo Metropolitan Institute of Medical Science; Bunkyo-ku, Tokyo, Japan

ARTICLE INFO

*Article history:*
Received 4 December 2008
Received in revised form 24 January 2009
Accepted 27 January 2009
Available online 6 February 2009

*Keywords:*
Autophagy
Neurodegeneration
Neurodegenerative disease
Axon
Axonopathy
Autophagosome
Lysosome
Endosome
Endocytosis
Multiple vesicular bodies (MVB)
ESCRT
p62/SQSTM1
Beclin 1
Protein inclusion bodies
Axonal dystrophy
Degeneration

ABSTRACT

Autophagy is a tightly regulated cell self-eating process. It has been shown to be associated with various neuropathological conditions and therefore, traditionally known as a stress-induced process. Recent studies, however, reveal that autophagy is constitutively active in healthy neurons. Neurons are highly specialized, post-mitotic cells that are typically composed of a soma (cell body), a dendritic tree, and an axon. Despite the vast growth of our current knowledge of autophagy, the detailed process in such a highly differentiated cell type remains elusive. Current evidence strongly suggests that autophagy is uniquely regulated in neurons and is also highly adapted to local physiology in the axons. In addition, the molecular mechanism for basal autophagy in neurons may be significantly divergent from "classical" induced autophagy. A considerable number of studies have increasingly shown an important role for autophagy in neurodegenerative diseases and have explored autophagy as a potential drug target. Thus, understanding the neuronal autophagy process will ultimately aid in drug target identification and rational design of drug screening to combat neurodegenerative diseases.



## 1. Introduction

Autophagy is a conserved lysosomal degradation pathway. In mammals, three types of autophagy have been described: macroautophagy, microautophagy and chaperone-mediated autophagy (CMA). These three types of autophagy differ in their mode of delivery of their substrates to lysosomes for degradation [1]. While little is known about the microautophagy process, a large body of studies has contributed to the current understanding of the macroautophagy and CMA pathways. Macroautophagy is the prototype of autophagy involving formation, delivery, and degradation of autophagic vacuoles (also called autophagosomes) through lysosomes, and will be the only form discussed in this review (hereafter referred to as autophagy). Although autophagy occurs in virtually all cell types, and likely involves highly conserved molecular machinery, emerging evidence suggests cell type/tissue-specific regulation of autophagy.

Neurons were one of the few cell types that were used in the initial identification and characterization of autophagy. With early access to electron microscopy (EM) in the last century, Alex Novikoff, Christian De Duve, and colleagues discovered and described the cell "self-eating" process of autophagy in the form of distinct vacuoles through ultrastructural analysis [2,3]. The formation of the autophagosomes, which engulfed a portion of cytoplasm and occurred in a large number, especially following axotomy and excitotoxic insult to neurons, is associated with "chromatolysis", a phenomenon that describes the area in neuronal cytoplasm that is devoid of organelles and filled with various types of vesicles [4]. These initial observations of neuronal autophagic activity were followed by a series of EM studies that revealed the accumulation of autophagosomes in the neurons of several human neurodegenerative diseases, including Alzheimer's disease (AD), Parkinson's disease (PD) and Huntington's disease (HD). With little knowledge of autophagic process and regulation, especially in mammalian tissues, neuronal autophagy, marked by elevated levels of autophagosomes, was viewed traditionally as a cellular mechanism that was highly destructive, and therefore was suspected to be a driving force in cell death [5].

* Corresponding author. Tel.: +1 212 241 3155; fax: +1 212 348 1310.
*E-mail address:* zhenyu.yue@mssm.edu (Z. Yue).

0167-4889/$ – see front matter © 2009 Elsevier B.V. All rights reserved.
doi:10.1016/j.bbamcr.2009.01.016

The arrival of the molecular era of autophagy study provided important evidence showing that autophagy is a primary stress response for cell survival. For example, loss-of-function studies demonstrate the essential role for autophagy-associated genes in the removal of "obsolete" proteins and organelles, thus protecting cell or neuron survival [6,7]. Therefore, in injured neurons or neurons bearing disease-related genes, altered autophagy, associated with increased numbers of autophagosomes, can be viewed as a beneficial response of neurons in repairing or remodeling damaged cellular components necessary for sustaining normal neuronal function and survival. However, other studies also provide genetic and cellular evidence that otherwise argues for a role of autophagy in promoting neuronal death, especially in neurons with acute injury [8].

More recent studies have begun to dissect the autophagic process in neurons under various stress or pathological conditions. These studies suggest that, while accumulation of autophagosomes can arise from increased production in some cases [9], it can be caused by a mechanism that blocks fusion and degradation of autophagosomes through lysosomes in other scenarios [10]. Given the current studies exploring the potential of autophagy as a drug target for the treatment of neurodegenerative diseases, a thorough investigation of the detailed mechanism whereby autophagy participates in each disease condition, would be critical for designing therapeutic intervention and evaluating the efficacy of an "autophagy drug" [11].

Over the past several years, characterization of autophagy in mammalian cells and animal models has greatly advanced our knowledge of the autophagy process in mammals. However, despite the recent effort and exponential growth in autophagy research as a whole, the progress in understanding the basic process and regulation of neuronal autophagy remains relatively slow. Recent studies have revealed the connections between autophagy and major neurological disorders such as (AD), (PD), and (HD) [12–14]. A common theme emerging in those studies is the role of autophagy in degrading disease-related, aggregate-prone mutant proteins such as tau, huntingtin and alpha-synuclein [15]. In addition, specific pathogenic mechanisms of AD, PD, or HD may profoundly alter autophagic activity. For example, while "inappropriate" autophagic induction may contribute to the increased synthesis of β-amyloid (Aβ) [16], blocked autophagic clearance is also implicated in cytotoxicity in AD [10]. Recently, genetic animal models containing reduced autophagic activity were used to examine the role of autophagy in the pathogenesis of AD, HD, and PD. These studies provided important evidence linking dysfunctional autophagy to the specific disease process [17,18], Friedman and Yue, unpublished). Due to numerous recent reviews on the study of autophagy in PD, AD, or HD [12–14,19–21], this review will instead summarize recent research in understanding the basis of neuronal autophagy, especially in primary neuronal cultures and the nervous system of animal models, and autophagic activity associated with other types of neuropathological conditions. Although limited and sometimes conflicting in their current forms, these studies nonetheless begin to shed light on specific cellular pathways and the connection of the physiological function of autophagy to disease mechanism.

## 2. Biosynthesis of autophagosomes is conserved from yeast to human

Morphological evidence for autophagy was first reported in the 1960s [3], but the underlying molecular mechanisms were not elucidated for another three decades. In the early 1990s, genetic screens of yeast mutants identified a number of *a*utophagy-related (*ATG*) genes essential for the autophagic molecular machinery [22,23]. Currently, 31 autophagy genes are known, many of which are required for autophagosome formation, at the nucleation, elongation, and/or fusion steps. Upon induction, an isolation membrane or phagophore forms and elongates, enveloping a portion of the cytosol, and encloses to form a double-membrane vacuole. Its outer membrane subsequently fuses with the lysosome, where its contents, together with the inner membrane, are digested by acidic hydrolases within the lysosomes (Fig. 1). Up to now, at least 14 mammalian homologues of yeast *ATG* genes have been identified, and characterization of their functions suggests that the autophagic machinery is highly conserved in mammals [24].

Studies in yeast revealed that, unlike endosomes and secretory vesicles, autophagosome formation does not require budding from existing organelles as its membrane source. Rather, autophagosomes may form from *de novo* membrane cisternae in the pre-autophagosomal structure (PAS), which contains several Atg protein complexes, and resides adjacent to the yeast vacuole [25–27]. It was shown that Atg9, the only known integral membrane protein associated with autophagic membranes, shuttles between a peripheral site in the cytoplasm and the PAS, therefore regulating the delivery of membrane to the PAS for expansion [27,28]. The Atg1 kinase complex, which contains regulatory subunit, Atg13, is involved in the retrieval of Atg9 from the PAS and is required for autophagosome formation [28,29]. Interestingly, the mammalian homologue of Atg9 (mAtg9) was shown to cycle between the trans-Golgi network (TGN) and late endosomes, which may serve as sources for membrane elongation. Starvation or rapamycin treatment induced redistribution of mAtg9 from TGN to peripheral late endosome membranes. Knock-down of Atg1 human homolog, ULK1, prevented this starvation-induced redistribution, suggesting that mAtg9 trafficking is ULK1-dependent [30].

In addition to the recruitment of membranes, Atg9 may also play a role in assembling protein complexes at the PAS [31]. Vps34, a class III phosphatidylinositol (PtdIns) 3-kinase mediates vesicular trafficking through its interactions with Vps15 and Atg6, and forms two distinct complexes: one with Atg14, which regulates autophagy-specific function, and the other with Vps38, for endosome-to-Golgi trafficking [32]. The PtdIns 3-kinase complex produces phosphatidylinositol 3-phosphate (PtdIns(3)P) which may recruit effector proteins, such as the Atg18–Atg2 complex, and together, both complexes are essential for nucleation [25]. The mammalian homologues of Vps34, Vps15 and Atg6 are hVps34, p150 and Beclin 1, respectively. Recent studies have found additional proteins that interact with the hVps34–p150–Beclin 1 complex: UVRAG [33], Atg14L (putative yeast Atg14 homologue) [34] and Rubicon [35]. These studies suggest the existence of multiple hVps34–Beclin 1 kinase complexes, which are involved in specific membrane trafficking mechanisms, including autophagy [35].

Two ubiquitin-like conjugation systems mediate autophagic membrane elongation; one involving the conjugation of Atg5 with Atg12 [36] and the other involving the covalent linkage of Atg8 with phosphatidylethanolamine (PE) [37]. Both Atg12 and Atg8 modifications share a single E1-like activating enzyme, Atg7, but are processed by two separate E2-like conjugating enzymes; Atg10 and Atg3 respectively [38]. The two ubiquitin-like conjugation systems are highly conserved from yeast to mammals [36,39]. The majority of Atg5 and Atg12 exists in the conjugated form and interacts noncovalently with multimeric protein, Atg16, in yeast and its functional counterpart, Atg16L, in mammals [40]. In one of the first studies linking the small GTPase Rab family to Atg proteins, Atg16L was shown to directly interact with Golgi-resident Rab33 and modulates autophagosome formation [41]. The Atg5–Atg12·Atg16 complex is essential for autophagosome formation and facilitates Atg8 conjugation with PE [40] through E3-like activity of Atg5–Atg12 for Atg8 conjugation [42].

Microtubule-associated protein 1 light chain 3 (LC3) is a mammalian homolog of yeast Atg8 and is cleaved at its C-terminal region by cysteine protease Atg4. This processed form (LC3-I) resides in the cytoplasm until it undergoes two ubiquitin-like modifications to become covalently linked to PE. Both the lipidated form LC3 (termed LC3-II) and Atg12–Atg5·Atg16 are recruited to the isolation membrane [38]. Whereas Atg12–Atg5·Atg16 dissociates upon autophagosome completion, LC3-II remains coupled to the autophagic

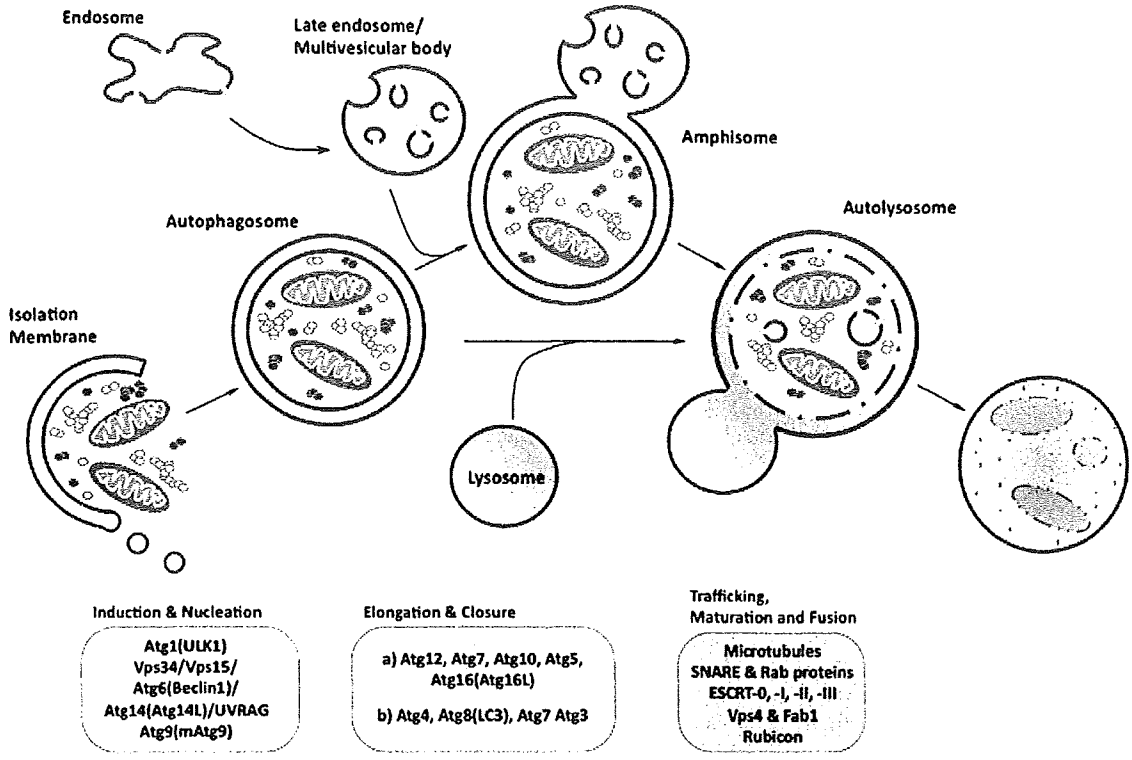


**Fig. 1.** A schematic representation of the macroautophagy process. Following induction, a phagophore or isolation membrane is formed. This process is regulated by Atg1 (Ulk1), Atg9, and the PtdIns 3-kinase complex, which includes Beclin 1, Atg14L, and UVRAG (nucleation). Two ubiquitin-like conjugation systems, which produce Atg8-PE (LC3II) and Atg5–Atg12, mediate the elongation of the isolation membrane, closure, and the formation a double-membrane vacuole known as the autophagosome. Autophagosomes can undergo maturation and fusion with early and late endosomes and MVBs, to generate the amphisome, followed by fusion with lysosomes, to form the autolysosome. Trafficking, maturation, and fusion events are mediated by microtubules and specific SNARE and Rab proteins. ESCRT proteins are also essential for MVB fusion with autophagosomes. Alternatively, immature autophagosomes can fuse directly with lysosomes.

membrane until fusion with the lysosome [39]. Prior to this fusion event, autophagosomes undergo a maturation process involving fusion with early and late endosomes, including multivesicular bodies (MVB), to form amphisomes [43]. Subsequently, these vacuolar bodies can then fuse with lysosomes to form the autolysosome (Fig. 1). These fusion events are mediated by SNARE proteins and Rab proteins, specifically Rab7, which is essential for maturation [44,45].

## 3. Neuronal autophagy: process and function in health and disease

### *3.1. Basal level autophagy*

#### *3.1.1. Unique feature of neuronal autophagy: scarcity of autophagosomes*

Previous studies using mice expressing an autophagosome marker, green fluorescent protein-tagged LC3 (GFP-LC3), suggested that autophagy is distinctly regulated in different tissues [46]. For example, food limitation triggers a rapid upregulation of autophagy in liver and heart as indicated by the formation of a large number of GFP-LC3-associated autophagosomes, whereas it fails to induce GFP-LC3-labeled autophagosomes in the CNS, despite the strong expression of GFP-LC3 in many types of neurons. In addition, LC3 exists predominantly in a soluble form (LC3-I) in healthy neurons, and levels of the lipidated form (LC3-II) do not change after starvation [46]. Recently, we have investigated the localization of GFP-Atg5, a green fluorescent Atg5 fusion protein used for monitoring isolation membrane, in CNS neurons of transgenic mice [47], and the results show that like GFP-LC3, GFP-Atg5 is largely diffuse regardless of whether food is available or withdrawn (Yue, unpublished data). Indeed, ultrastructural analysis also confirmed scarcity of double-membrane vacuoles that are characteristic of autophagosomes in healthy neurons [48]. In contrast, many tissues, including liver and heart, have many GFP-LC3 puncta even when food is not limited, thus providing direct evidence for constitutively active autophagy under normal conditions.

The above evidence suggests that neurons normally maintain low levels of autophagosomes, and perhaps a low rate of autophagosome biosynthesis, even with the fluctuation of available nutrients. The current hypothesis is that neurons are prohibited from large-scale autophagy induction in response to starvation due to their ability to utilize multiple energy sources to maintain normal neuronal function. For example, glial cells provide nutrient and neurotrophin support to neurons and peripheral organs supply necessary nutrients to the CNS under hypothalamic regulation [49]. Thus, it is possible that even after 48 h of fasting in mice, it is insufficient to cause nutrient or trophic factor depletion in the CNS neurons due to compensatory mechanisms of nutrient supply. Interestingly, without showing the availability of nutrient or trophic factors, a recent study reported that mTOR activity (an important regulator of autophagy) was significantly reduced, at least in hypothalamic neurons, after 48 h of starvation in mice [50]. Despite the reduced mTOR activity, there was no report of the formation of GFP-LC3 or GFP-Atg5 puncta in hypothalamic neurons (Yue, unpublished data), [46]. While the mTOR activity in hypothalamic neurons of GFP-LC3 or GFP-Atg5 transgenic mice after 48 hour-starvation remains to be determined, other studies observed mTOR-independent regulation of autophagy in neurons [51,52]. Importantly, Young et al., showed that insulin plays a critical role in suppressing the induction of autophagy in primary neuron cultures. Through screening culture medium components, they found that insulin (but not other components, including amino acids) was the key factor and that

the absence of insulin induced autophagy in primary neurons, in an mTOR-dependent manner. Surprisingly, a highly potent Akt inhibitor also efficiently induces autophagy, however, via an mTOR-independent pathway [51]. This result suggests that the active insulin signaling is responsible for the low level of autophagosome formation in healthy neurons, and therefore, the insulin pathway may provide a critical mechanism for controlling basal autophagy in neurons. Although the autophagy control mediated by insulin signaling is not restricted to neurons [53], it can be adapted to the neuronal physiology that is related to the high consumption of energy via distinct sources. In addition, multiple parallel signaling pathways, including the mTOR pathway, exist in neurons to regulate autophagy.

Apart from the insulin pathway, specific proteins or protein modifications expressed in neurons may also contribute to additional regulation of basal autophagy in neurons. Previously, we showed that expression of a microtubule associated protein 1B (MAP1B), which is enriched in neurons and binds LC3 with high affinity, remarkably affects the formation of GFP-LC3 puncta (autophagosomes), and this effect is dependent on the status of certain modifications of MAP1B [54], (see section 4.2 of this review).

Taken together, we propose that the regulation of basal autophagy in CNS neurons at least involves the following mechanisms: (1) a non-cell-autonomous mechanism whereby nutrients, hormones (insulin), or neurotrophic factors are supplied by peripheral organs or glial cells, (2) a cell-autonomous control mechanism by intrinsic nutrient-mediated signaling or specific factors expressed in neurons. Furthermore, current evidence also raises the question as to what context or extent does mTOR-mediated signaling regulates autophagy in neurons.

While the hypothesis for the low level of basal autophagy (in the form of "classical" autophagosomes) and its regulation remains to be tested further, a recent study provides evidence suggesting an alternative hypothesis that autophagosomes, once formed, are rapidly cleared by fusion with lysosomes in primary neuronal culture. It further proposes that the clearance of autophagosomes by basal autophagy is highly efficient in neurons and accounts for the low levels of autophagosomes [10]. Apparently, future experiments focused on directly measuring or imaging the dynamics of autophagy flux will be needed to solve this issue.

#### 3.1.2. Essential role of basal autophagy in cellular homeostasis and neuroprotection

Current evidence suggests that neuronal autophagy is tightly regulated and autophagosomes are maintained at minimal levels. However, recent studies in mutant mice with targeted deletion of *Atg5* or *Atg7* specifically in brain, unequivocally demonstrate the importance of basal autophagy in CNS neurons [6,7]. Unlike *Atg5*- or *Atg7*-deficient yeast or mammalian MEF cells that survive and grow normally with regular culture conditions, CNS neurons lacking *Atg5* or *Atg7* in animal models undergo progressive degeneration, even when mice are housed under normal conditions. Importantly, *Atg5* or *Atg7* deficient neurons develop a massive number of inclusion bodies that are labeled by ubiquitin, suggesting that continuous autophagy is required to prevent the build-up of intracytoplasmic protein aggregation. These studies provide undeniable proof for the existence and critical function of basal autophagy in neurons. Paradoxically, the evidence that autophagy is in continuous action through autophagosome–lysosome degradation is at odds with the scarcity of autophagosomes or low level of basal autophagy in the healthy neurons. Although it appears to be consistent with the hypothesis of highly efficient basal autophagy [10], an alternative hypothesis is that basal autophagy in neurons proceeds via a distinctive mechanism (e.g. in the absence of "classical" autophagosomes formation). Even though autophagy genes (ATG system) are required, they participate in the lysosomal degradation pathway that differs from canonical autophagy (in the presence of well-documented autophagosome formation) [55]. One well-known example for such an autophagy-related cellular process, is the yeast Cvt (cytoplasm-to-vacuole targeting) pathway, which shares most of its protein components with autophagy, but is biosynthetic and functions to specifically deliver certain enzymes to vacuoles [56]. Future studies should investigate the possibility of non-canonical or adapted autophagy in neurons.

Although CNS neurons are generally vulnerable to the loss of the autophagy pathway, the degree of vulnerability and the formation of intracellular inclusions vary significantly among different neuron types as observed in the mutant brains deficient in *Atg5* or *Atg7*. The ablation of the *Atg5* or *Atg7* gene may trigger a cell-type specific cellular response to autophagy deficiency and/or a cell type-dependent mechanism contributing to the neurotoxicity. For example, Purkinje cells deficient in *Atg5* or *Atg7* display very few ubiquitin-associated inclusions, whereas these cells are among the most vulnerable neuron types [57,58]. In contrast, a large number of ubiquitin-associated inclusions are seen in the brain region where neuronal loss was hardly detected when autophagy was genetically inhibited (Waguri S, Komatsu M, unpublished data). While it is possible that the compensatory pathways to the loss of autophagy vary in different neuronal types and account for the difference in their vulnerability, it may also reflect the disparity in their intrinsic demands for autophagy, as well as relative levels of basal autophagy. Neurons exposed to high levels of various stresses may contain high levels of basal autophagy and are therefore, far more vulnerable, whereas the neurons that require low levels of basal autophagy through their lives are relatively resistant to autophagy deficiency.

### 3.2. Induced autophagy in neurons: signaling and distinctive stress response

The primary function of autophagy is to provide cellular response to nutrient limitation by mobilization of autophagosome–lysosome degradation pathway. A large body of evidence shows that nutrient-related signaling pathways regulate autophagic activity in mammals. These pathways include insulin and amino acid pathways, mTOR kinase complex [59–61], AMP-activated protein kinase (AMPK) [62] and Beclin 1/Vps34 (class III PI-3 kinase, PtdIns3K) lipid kinase complex [63]. Despite the growing evidence linking these signaling pathways to autophagy regulation, the details for how they control the complex process of autophagy is lacking. Furthermore, little is known about tissue/cell type-dependent regulation. A recent study in primary cortical neuronal culture shows that insulin plays a critical role in controlling the induction of autophagy [51].

A unique feature of neurons, with respect to their fuel supply, is that they use glucose (or ketones) almost exclusively as a blood-borne energy substrate to provide energy and carbon chains for protein synthesis. Therefore, compared to other tissues/cell types, CNS neurons may depend less on autophagy to provide free amino acids or energy under physiological conditions. It can be further speculated that the primary function of neuronal autophagy at the basal level is different than as a primary nutrient-starvation response [49]. Accordingly, neurons are likely to use a distinctive mechanism for autophagy regulation. Adding to the complexity of autophagy regulation in neurons, a recent study shows that cultured neurons from male rats more readily undergo autophagy in response to 24 h of nutrient deprivation compared to female neurons [64], indicating gender differences in autophagic capacity of neurons.

While nutrient-related pathways are likely the conserved mechanism for the control of neuronal autophagy [10,51], the direct *in vivo* evidence that these pathways contribute to the induction of autophagy (e.g. synthesis of a large number of autophagosomes) in CNS neurons remains to be shown. Despite the lack of *in vivo* evidence of neuronal autophagy mediated by nutrient signaling, recent studies in animal models indicate that, in contrast to nutrient starvation which rarely induces autophagy, a variety of stress-related signals,

nature
REVIEWS
ebruary 2009 volume 10 no. 2
www.nature.com/reviews

# MOLECULAR CELL BIOLOGY

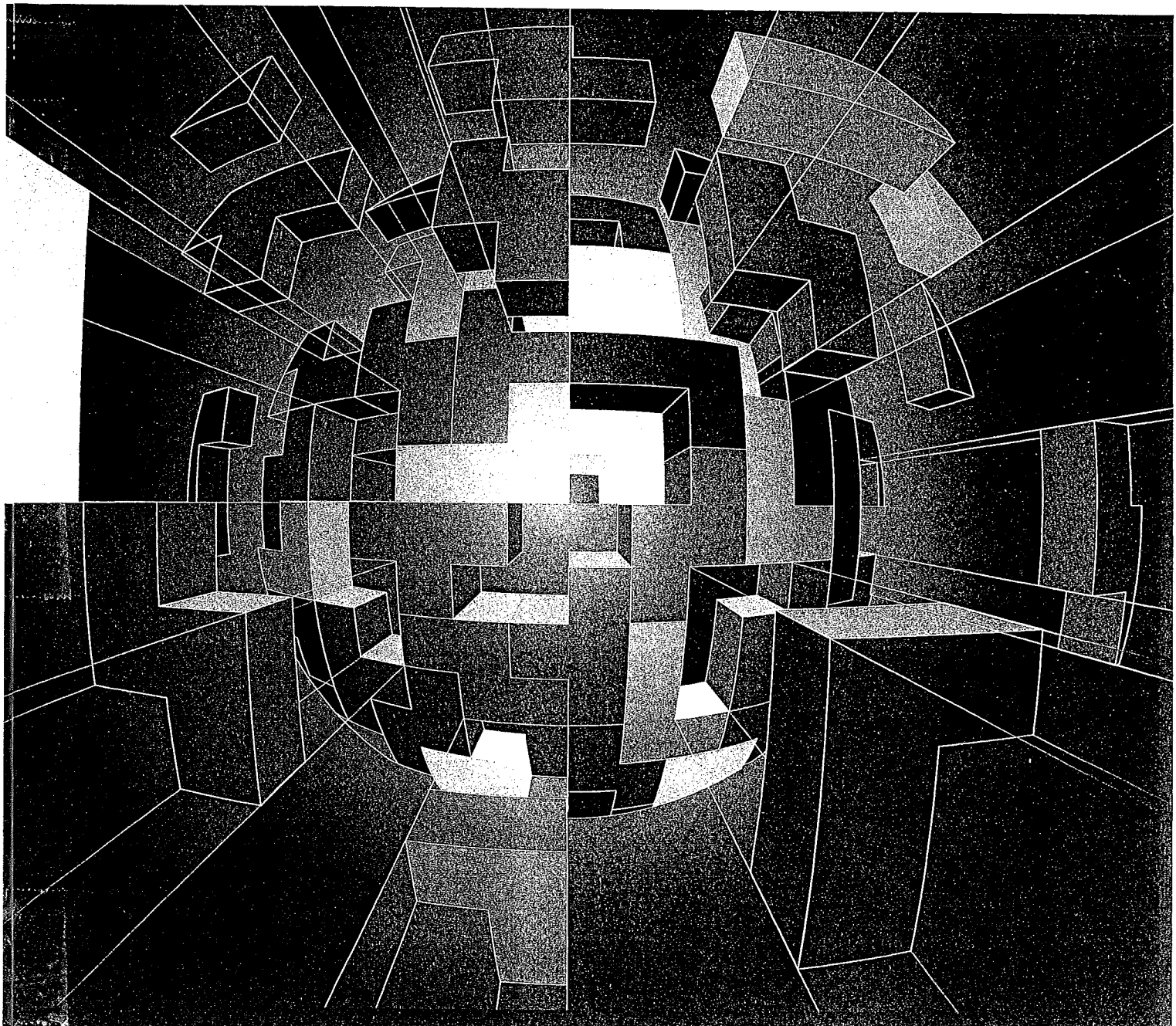

MICRORNA TARGETING
General principles are challenged under *in vivo* conditions

Establishing the body plan

# Molecular mechanisms of proteasome assembly

*Shigeo Murata*, Hideki Yashiroda* and Keiji Tanaka‡*

Abstract | The 26S proteasome is a highly conserved protein degradation machine that consists of the 20S proteasome and 19S regulatory particles, which include 14 and 19 different polypeptides, respectively. How the proteasome components are assembled is a fundamental question towards understanding the process of protein degradation and its functions in diverse biological processes. Several proteasome-dedicated chaperones are involved in the efficient and correct assembly of the 20S proteasome. These chaperones help the initiation and progression of the assembly process by transiently associating with proteasome precursors. By contrast, little is known about the assembly of the 19S regulatory particles, but several hints have emerged.

Caspase-like activity
Enzymatic activity that is similar to that of caspases — Cys proteases that have essential roles in apoptosis. β1 was first reported to cleave after Glu residues, and was thus termed peptidylglutamyl peptide hydrolase. Later, it was found that β1 also cleaves after Asp acid residues in substrates of caspases.

**Laboratory of Protein Metabolism, Department of Integrated Biology, Graduate School of Pharmaceutical Sciences, The University of Tokyo, 7-3-1 Hongo, Bunkyo-ku, Tokyo 113-0033, Japan.*
*‡Laboratory of Frontier Science, Tokyo Metropolitan Institute of Medical Science, 3-18-22 Honkomagome, Bunkyo-ku, Tokyo 113-8613, Japan.*
*Correspondence to K.T.*
*e-mail:*
*tanaka-kj@igakuken.or.jp*
doi:10.1038/nrm2630

The 26S proteasome is a eukaryotic ATP-dependent protease that is known to collaborate with the ubiquitin system — the system that tags proteins with polyubiquitin chains as a marker for protein degradation in eukaryotic cells[1,2] (BOX 1). The 26S proteasome is involved in a diverse array of biological processes, including cell-cycle progression, DNA repair, apoptosis, immune response, signal transduction, transcription, metabolism, protein quality control and developmental programmes. It catalyses the precise, rapid and timely degradation and, thus, the irreversible inactivation of targeted proteins. This ensures unidirectional progression of such biological processes.

The 26S proteasome is an unusually large protein complex that consists of two portions: the catalytic 20S proteasome of approximately 700 kDa (also called the 20S core particle (CP)) and the 19S regulatory particle (RP; also called PA700) of approximately 900 kDa, both of which are composed of a set of multiple distinct subunits[1,3] (FIG. 1).

The eukaryotic 20S proteasome is a cylindrical particle that is formed by axial stacking of four heteroheptameric rings — two outer α-rings and two inner β-rings, each comprising seven structurally similar α- and β-subunits, respectively. β-rings form a proteolytic chamber and α-rings serve as a gate for entry into the chamber (FIGS 1,2). Of these 14 subunits, β1, β2 and β5 subunits have hydrolytic activity as Thr proteases for the cleavage of peptide bonds at the carboxyl-terminal side after acidic, basic and hydrophobic residues, respectively. These activities are referred to as caspase-like activity (or peptidylglutamyl-peptide hydrolysing activity), trypsin-like activity and chymotrypsin-like activity, respectively[4,5]. The active sites of the catalytic β-subunits are located on the inner surface of the proteolytic chamber[6,7].

The 19S RP consists of at least 19 different subunits and can be divided into two subcomplexes: the base and the lid[3,8,9] (FIG. 1). The base is composed of six different homologous AAA+ ATPase subunits, regulatory particle triple-A protein 1 (RPT1)–RPT6, and three non-ATPase subunits, regulatory particle non-ATPase 1 (RPN1), RPN2 and RPN13 (REFS 8,10–14). The ATPase subunits are required for substrate unfolding and α-ring channel opening, which are prerequisites for threading substrates into the 20S proteasome. RPN1, RPN13, RPT5 and RPN10 capture ubiquitylated proteins either directly or through proteins that contain both UBL (ubiquitin-like) domains and UBA (ubiquitin-associated) domains, such as radiation sensitive 23 (RAD23), dominant suppressor of Kar1 2 (DSK2) and DNA-damage-inducible 1 (DDI1)[3,8,15–20]. RPN10 is assumed to sit at the interface of the lid and base. The lid is composed of nine non-ATPase subunits: RPN3, RPN5–RPN9, RPN11–RPN12 and RPN15 (also called SEM1; DSS1 in mammals)[8,21,22]. The one defined biochemical activity of the lid is the de-ubiquitylation of captured substrates to facilitate their degradation, a process in which the metalloisopeptidase RPN11 has an essential role[23–25]. However, the functions of the other subunits remain unknown. The 19S RP is attached at one or both ends of the 20S proteasome, forming the 26S proteasome. The 26S proteasome acts as an efficient and exhaustive shredder of proteins in living cells. The 19S RP selects proteasomal substrates through